Atmos. Chem. Phys., 15, 11885–11907, 2015
www.atmos-chem-phys.net/15/11885/2015/
doi:10.5194/acp-15-11885-2015

Atmospheric Chemistry and Physics
Open Access
EGU

Black carbon surface oxidation and organic composition of beech-wood soot aerosols

J. C. Corbin[1,a], U. Lohmann[1], B. Sierau[1], A. Keller[2], H. Burtscher[2], and A. A. Mensah[1]

[1]ETH Zurich, Institute for Atmospheric and Climate Science, Zurich, Switzerland
[2]Institute of Aerosol and Sensor Technology, University of Applied Sciences Northwestern Switzerland, Windisch, Switzerland
[a]now at: Laboratory for Atmospheric Chemistry, Paul Scherrer Institute, Villigen, Switzerland

Correspondence to: J. C. Corbin (joel.corbin@psi.ch) and A. A. Mensah (amewu.mensah@env.ethz.ch)

Received: 9 February 2015 – Published in Atmos. Chem. Phys. Discuss.: 31 March 2015
Revised: 15 September 2015 – Accepted: 24 September 2015 – Published: 26 October 2015

Abstract. Soot particles are the most strongly light-absorbing particles commonly found in the atmosphere. They are major contributors to the radiative budget of the Earth and to the toxicity of atmospheric pollution. Atmospheric aging of soot may change its health- and climate-relevant properties by oxidizing the primary black carbon (BC) or organic particulate matter (OM) which, together with ash, comprise soot. This atmospheric aging, which entails the condensation of secondary particulate matter as well as the oxidation of the primary OM and BC emissions, is currently poorly understood.

In this study, atmospheric aging of wood-stove soot aerosols was simulated in a continuous-flow reactor. The composition of fresh and aged soot particles was measured in real time by a dual-vaporizer aerosol-particle mass spectrometer (SP-AMS). The dual-vaporizer SP-AMS provided information on the OM and BC components of the soot as well as on refractory components internally mixed with BC. By switching the SP-AMS laser vaporizer off and using only the AMS thermal vaporizer (at 600 °C), information on the OM component only was obtained. In both modes, OM appeared to be generated largely by cellulose and/or hemicellulose pyrolysis and was only present in large amounts when new wood was added to the stove. In SP-AMS mode, BC signals otherwise dominated the mass spectrum. These signals consisted of ions related to refractory BC (rBC, C^+_{1-5}), oxygenated carbonaceous ions (CO^+_{1-2}), potassium (K^+), and water (H_2O^+ and related fragments). The $C^+_4 : C^+_3$ ratio, but not the $C^+_1 : C^+_3$ ratio, was consistent with the BC-structure trends of Corbin et al. (2015c). The CO^+_{1-2} signals likely originated from BC surface groups: upon aging, both CO^+ and CO^+_2 increased relative to C^+_{1-3} while CO^+_2 simultaneously increased relative to CO^+. Factor analysis (positive matrix factorization) of SP-AMS and AMS data, using a modified error model to address peak-integration uncertainties, indicated that the surface composition of the BC was approximately constant across all stages of combustion for both fresh and aged samples. These results represent the first time-resolved measurements of in situ BC surface aging and suggest that the surface of beech-wood BC may be modelled as a single chemical species.

1 Introduction

Soot particles formed during the combustion of organic fuels are a major source of particulate matter (PM) from diesel engines, open burning, and biofuel heating and cooking (Bond et al., 2013). The black carbon (BC) in soot particles is highly light absorbing, with a radiative forcing potentially comparable to CO_2 (Ramanathan and Carmichael, 2008; Bond et al., 2013). However, the magnitude of the radiative absorption remains highly uncertain due to uncertainties related to the role of atmospheric coatings of non-refractory PM (NR-PM) on BC-containing particles. Such coatings may enhance light absorption (Jacobson, 2001; Mikhailov et al., 2006), cloud interactions (Kuwata et al., 2009; Liu et al., 2013), and/or alter the deposition rates and thus atmospheric distribution (Liu et al., 2011; Bond et al., 2013) of BC-containing particles. The formation and composition of coatings on soot

particles is therefore a topic of major current interest (Cappa et al., 2012, 2013; Jacobson, 2013; Liu et al., 2013).

In addition to their role in climate, freshly formed soot particles have been associated with negative impacts on vascular, cardiopulmonary, and respiratory health (Lighty et al., 2000; Brook et al., 2010; Heal et al., 2012) as well as lung cancer (Attfield et al., 2012; Silverman et al., 2012). Multiple studies have shown that ozonolysis enhances the apparent toxicity of soot or BC particles (Klippel and Nussbaumer, 2007; Holder et al., 2012; McWhinney et al., 2011; Li et al., 2013). However, the mechanisms behind these effects remain unclear. While the organic PM component (OM) may play a role (McWhinney et al., 2011), BC toxicity generally persists after washing in both polar and non-polar solvents (Pan et al., 2004; McWhinney et al., 2013). This suggests that the responsible species are either very strongly adsorbed or chemically contiguous with the BC surface (McWhinney et al., 2013); we refer to these species as "BC surface groups". The composition of such surface groups is expected to vary widely between samples, fuel type, and combustion conditions (Kolb et al., 2010).

BC surface groups are formed during in-flame oxidation (Stanmore et al., 2001; Tree and Svensson, 2007; Glassman and Yetter, 2008) or reaction with O_2 or other oxidants soon after emission (Stanmore et al., 2001; Glassman and Yetter, 2008). Offline analyses have measured oxygenated BC surface groups on BC from diesel engines, aircraft turbines, wood combustion, diffusion flames, and even particles formed after the spark vaporization of graphite in argon (Akhter et al., 1985a, b; Smith and Chughtai , 1995; Vernooij et al., 2009; Zelenay et al., 2011; Daly and Horn, 2009; Han et al., 2012a; Corbin et al., 2015c). These surface groups have been identified as containing C=O, C−O−C, and/or C−OH groups using FTIR (Smith and Chughtai , 1995; Hopkins et al., 2007; Daly and Horn, 2009; Cain et al., 2010; Han et al., 2012a, b, 2013) and NEXAFS (Hopkins et al., 2007; Vernooij et al., 2009; Zelenay et al., 2011).

The ubiquity of oxygenated surface groups on fresh BC surfaces does not mean that fresh soot particles will appear hydrophilic on a macroscopic scale. For example, fresh soot particles do not generally activate as cloud-condensation nuclei (CCN) under atmospherically relevant conditions (e.g., Tritscher et al., 2011). Instead, BC surface groups may present sites for molecular adsorption, with consequences for the heterogeneous chemistry of soot particles (Alcala-Jornod and Rossi, 2004). This heterogeneous chemistry includes the health effects discussed above, as well as the reaction of soot particles with trace gases in the atmosphere (Kolb et al., 2010). In particular, the heterogeneous reaction of photoactivated BC surface species with NO_2 and surface-adsorbed H_2O may produce enough HONO to contribute significantly to OH concentrations in the urban atmosphere (Monge et al., 2010).

In addition to BC, aerosols emitted by combustion commonly contain OM and inorganic ash (Lamberg et al., 2011; Torvela et al., 2014). Combustion-emitted organics are a major global source of primary OM from both natural and anthropogenic sources (Bond et al., 2004, 2013) and may vary widely in composition depending on the fuel and combustion process. For biomass combustion in particular, the composition of OM varies considerably between fuels and combustion conditions (Shafizadeh, 1984; Simoneit et al., 1993; Rogge et al., 1998; Fine et al., 2001; Weimer et al., 2008; Ortega et al., 2013). For example, the same fuel burnt in the same stove may emit organics of different composition and in different amounts, depending on factors such as air flow and stove temperature (Shafizadeh, 1984; Eriksson et al., 2014).

The organics emitted during biomass combustion are typically semivolatile (Lipsky and Robinson, 2006; Donahue et al., 2012) and partition dynamically between the gas and particle phases of an aerosol. Atmospheric oxidation of these organics may increase their degree of oxygenation, altering the ability of aerosol particles to take up water (Zelenay et al., 2011) and/or act as CCN (Engelhart et al., 2012). Oxidation may also lower the vapour pressures of primary organic emissions, decrease their vapour pressure, and lead to their condensation as OM within hours of emission (Akagi et al., 2012; Vakkari et al., 2014). Such OM enhancement has been consistently observed for aged wood-stove emissions (Grieshop et al., 2009; Heringa et al., 2011; Ortega et al., 2013; Corbin et al., 2015a). For open-biomass-burning emissions, OM enhancements are much more variable and often negligible (Hennigan et al., 2011; Jolleys et al., 2012).

Residential biomass combustion is a significant component of global anthropogenic combustion emissions (Bond et al., 2013) and has been named the largest OM source in Europe (Denier van der Gon, 2014). This OM, together with co-emitted BC, may dominate other wintertime pollution sources outside of cities (Szidat et al., 2006, 2007; Lanz et al., 2007; Fountoukis et al., 2014). Residential biomass combustion is commonly performed using logwood stoves (Fountoukis et al., 2014), which may produce particles with a toxicity comparable to or worse than that of diesel-exhaust particles for normal or poor combustion, respectively (Klippel and Nussbaumer, 2007). An understanding of the initial and aged composition of these pollutants is therefore essential for the understanding and regulation of their emission with regard to their health and climate effects.

This study evaluates the composition of BC and OM in soot formed by combustion in a modern wood stove both before and after simulated atmospheric aging. The stove was operated under optimal conditions using beech wood as the fuel. Beech is one of the major forest trees in Europe (Simpson et al., 1999; Brunet and Richnau, 2010), and its wood is commonly purchased or gathered for combustion as a heating or cooking fuel (Schmidl et al., 2008).

An online, dual-vaporizer soot-particle mass spectrometer was used to characterize the fresh and aged soot. As described in Sect. 2.2, the Soot-Particle Aerosol Mass Spectrometer (SP-AMS) vaporizer allowed entire soot particle

to be examined whereas the AMS vaporizer detected only the NR-PM component (mostly OM). Thus the coatings and composition of the soot could be studied. Data with the SP-AMS laser on are referred to as "SP-AMS measurements" below; with the laser off data are referred to as "AMS measurements".

The data were analyzed using two approaches. First, selected ions and representative mass spectra were investigated. Second, factor analysis was used to obtain 3–4 representative factors to allow the entire SP-AMS and AMS data sets to be succinctly described and compared. The results are then discussed in terms of BC surface oxidation, OM composition, potassium content, and particulate water content.

2 Methods

2.1 Experimental

The experimental setup used here has been detailed in Corbin et al. (2015a). Beech-wood logs (*Fagus sylvatica*) were burnt in a modern logwood stove (9 kW, Rüegg Mars, Switzerland) according to official Swiss type-approval protocols at the officially certified testing facility of the University of Northwestern Switzerland (Swiss register STS 396, European register NB 2113). The stove was operated by facility personnel resulting in burns that were, relative to household usage, extremely reproducible.

Wood logs were added to the stove in batches of ~ 3 kg (see inset of Fig. 3). The first batch of each measurement day was ignited using a small amount of tinder (a commercial product containing paraffin wax with the appearance of wood wool) and kindling (small pieces of wood). The tinder and kindling were placed on top of the first batch of wood logs, which therefore burnt top-down. Subsequent batches were allowed to self-ignite upon the embers of the previous batch, burning bottom-up. In both cases, the stove operator increased the airflow into the stove at the beginning of each burn to facilitate the onset of flaming combustion. The consequential increase in dilution was corrected for in Corbin et al. (2015a) but not herein, for reasons discussed below.

Wood-combustion emissions were directed through an indoor chimney where a heated sampling line (433 K) extracted samples for analysis. After eightfold dilution, samples were either measured as is, oxidized (see below), or filtered and oxidized for a given burn. The discussion below focusses on the first case (fresh emissions) and oxidized case (aged emissions).

Aging was performed using the Micro-Smog Chamber (MSC, Keller and Burtscher, 2012). The MSC is described in detail in Keller and Burtscher (2012) and Corbin et al. (2015a), so only a brief description is given here. The reactor consists of three UV-grade quartz tubes totalling only $\sim 225\,\mathrm{cm}^3$ in volume. Losses of particles and low-volatility gases to the UV-heated MSC walls are expected to be negligible (Corbin et al., 2015a). Aerosols entering the MSC are exposed to 4 W of UVC irradiation (254 nm and 185 nm emission lines) generated by five low-pressure mercury lamps (Heraeus, type GPH212T5VH/2), forming O_3 from O_2 and subsequently $OH^\bullet$ from background water vapour. In the second tube, 30 W of UVA radiates from a high-pressure halogen lamp (Panacol-Elosol, type UV-H 255) to drive further $OH^\bullet$ chemistry. Some NO_x ($= NO + NO_2$) or SO_2 chemistry is also possible depending on the combustion emissions. The last MSC tube allows the aerosol to cool slightly while reaction continues. Some experiments were performed with the intermediate UVA tube removed, resulting in no observed differences in this study (Corbin et al., 2015a). For this study, OH exposures were estimated at roughly $10^9\,\mathrm{molec\,cm^{-3}\,h^{-1}}$ based on follow-up experiments (Bruns et al., 2015). This represents an extreme upper limit for atmospheric OH exposure.

2.2 Soot-Particle Aerosol Mass Spectrometer

The SP-AMS used in this study is an HR-ToF-AMS (hereafter shortened to AMS) equipped with a switchable 1064 nm continuous-wave soot-particle vaporization module (Onasch et al., 2012). The SP module was switched on and off periodically, whereas the AMS vaporizer (described below) remained on continuously. Thus the data reported here represent either standard AMS measurements or dual-vaporizer SP-AMS measurements. Here, we use these terms to indicate the laser state where relevant, also referring to the instrument itself as the SP-AMS.

The design of the SP-AMS has been described in detail elsewhere (Onasch et al., 2012). In brief, the instrument samples aerosol through an aerodynamic lens, which efficiently focusses particles with aerodynamic diameters between approximately 60 and 600 nm into a narrow beam. The lens opens into a vacuum-pumped chamber, where gas expansion accelerates particles to their size-dependent terminal velocity. Particles then transit a sizing chamber to be vaporized within an ionization chamber. Vaporization is achieved by a switchable 1064 nm continuous-wave laser (SP-AMS mode) or by impaction upon a porous-tungsten thermal vaporizer held at 873 K (600 °C; AMS mode).

In SP-AMS mode, 1064 nm light-absorbing refractory PM (LR-PM) is heated to vaporization by the continuous-wave laser. Due to this heating, any internally mixed material which is refractory below the LR-PM vaporization temperature may also be vaporized. In this study, the LR-PM was rBC, which vaporizes at ~ 4000 K (Schwarz et al., 2006; Moteki and Kondo, 2010), so that NR-PM (here mostly OM; Corbin et al., 2015a), ash, or BC surface functionalities (Corbin et al., 2015c) are vaporized when internally mixed with rBC. NR-PM that is not internally mixed with rBC will pass through the SP-AMS laser and be vaporized on the AMS thermal vaporizer. In AMS mode, only NR-PM is vaporized. In both cases, the vapour is ionized by electron impact. The

resulting ions are mass analyzed by pulsed extraction into an ion-time-of-flight chamber.

The SP-AMS can provide free-molecular-regime aerodynamic-size measurements by modulating the sampled particle beam with a mechanical "chopper" and monitoring the time taken for signals to be observed (particle time-of-flight, or PToF, mode). In this study, PToF data were accumulated over 15–20 s min^{-1} and were further averaged before analysis. For the remainder of each minute, mass spectrum (MS) mode data were acquired by removing the chopper entirely ("open" position) for 5 s of particle-beam measurements, then replacing it entirely ("closed" position) for 5 s of background measurements. The closed signals were subtracted from the corresponding open signals after data analysis (described below). Using a camera, the laser was observed to stabilize after roughly 5 s when switching on (going from AMS to SP-AMS mode) and almost instantly when switching off (vice versa). So, since each chopper cycle began with a closed measurement (no rBC), no additional wait time was specified when switching the laser on or off. The ion-time-of-flight chamber was operated in single-reflectron "V" mode with a resolution of 4200 at m/z 91. This mode was sufficient for the unambiguous distinction and determination of elemental composition for virtually all ions, with exceptions discussed below. In SP-AMS mode, the instrument was operated in two separate mass-spectral configurations, one of which extended to 1000 m/z to monitor for the fullerene-ion signals that have been previously observed (Onasch et al., 2012; Fortner et al., 2012; Corbin et al., 2015c). No fullerenic signals were observed, so these data are not presented. Therefore, in the data presented below, one SP-AMS measurement is available for every two AMS measurements.

2.3 SP-AMS and AMS data analysis

Ion signals in the SP-AMS/AMS were identified and integrated using a modified version of the open-source PIKA software (version 1.10H; Sueper et al., 2011) as well as custom code written in Igor Pro (version 6.2 and 6.3; WaveMetrics, OR, USA). Two major modifications were made to PIKA. First, the robustness of the peak-shape and peak-width-calibration determinations were improved as described in the Supplement. Second, peak-integration uncertainties were estimated as discussed in Corbin et al. (2015b) and described briefly in Sect. 2.4.

2.3.1 CO^+ signals

Special attention was given to the ions H_xO^+ and CO^+, which are sensitive to interferences from background H_2O and N_2, respectively, and are normally estimated from the signal at CO_2^+ (Allan et al., 2004; Aiken et al., 2008).

CO^+ signals were directly quantified in PIKA as described in detail in Corbin et al. (2015a). That is, the height of an empirically defined pseudo-Gaussian peak was fitted simultaneously to each of CO^+ and N_2^+. The fitted pseudo-Gaussians were constrained in position by the m/z calibration and in width by a peak-width calibration. While these signals normally suffer from poor resolution from N_2^+, the current mass spectrometer was able to resolve the two peaks when CO^+ signals were very high (above 1000 counts per second; Corbin et al., 2015a). As shown in Figs. 1 and 2 and in more detail in Corbin et al. (2015a), the CO^+ fits resulted in reproducible CO^+ : CO^+ ratios for each experiment. In the aged experiment, this ratio was 1.22 ± 0.01 in the AMS; in the filtered-and-aged experiment not discussed herein (see Corbin et al., 2015a), this ratio was 0.86 ± 0.02 in the AMS. These values are consistent with literature-observed ratios of 0.9–1.25 (Aiken et al., 2008) and are discussed further in Corbin et al. (2015a). The possibility that other unidentified ions remained poorly resolved from N_2^+ is very unlikely, as also described in that publication.

2.3.2 Gas-phase interferences at CO^+ and at CO_2^+

Gas-phase interferences at CO_2^+ were corrected for using filtered-aerosol measurements taken periodically throughout each experiment. This method has been detailed by Collier and Zhang (2013). The CO_2^+ correction was smaller than that needed for atmospheric measurements due to the factor-of-200 dilution by synthetic air (80 % N_2, 20 % O_2, 99.999 % purity), and the correction factor was dynamically scaled by continuous gas-phase carbon-dioxide measurements. The resulting correction factor was 7–15 % of the measured CO_2^+ signals (interquartile range, both experiments) and depended on the stage of combustion.

Gas-phase interferences at CO^+ were not corrected for. The high modified combustion efficiency (MCE) during these experiments meant that CO(g) emissions were much smaller than CO_2(g) emissions, especially during the periods when CO^+ could be quantified. In particular, for the periods when CO^+ signals were high enough to be quantified (due to the peak-fitting limitations described above) the CO_2^+ correction factor was 0.6–2 % (interquartile range, both experiments). These periods corresponded to MCE values greater than 0.97, so the CO^+ correction factor would have been less than < 3 % of the CO_2^+ correction factor (note that CO^+ signals were generally higher than CO_2^+ when quantifiable). This correction would be negligible relative to the uncertainty in the CO^+ due to the fit described above.

2.3.3 Water signals

The ions H_xO^+ (= O^+, HO^+, and H_2O^+) were not quantifiable in MS mode due to interferences from background water. That these three ions originated from water, and not from the fragmentation of other molecules, was confirmed with the ratios of particulate (PToF) signals at O^+ : HO^+ : H_2O^+ (Aiken et al., 2008; Chen et al., 2011), which was 4 : 25 : 100

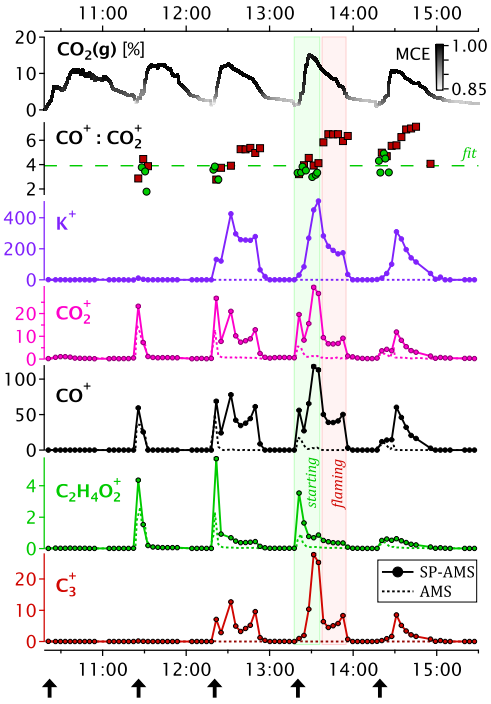

Figure 1. Time series for the fresh beech-wood-combustion experiment. Selected SP-AMS (solid lines with circles) and AMS (dashed lines) data are shown in nitrate-equivalent mass (proportional to ion counts). Error bars are smaller than the data symbols. The uppermost panel shows gas-phase CO_2(g) concentrations in the chimney (proportional to combustion rate), shaded by the modified combustion efficiency (MCE). The second-from-top panel shows the $CO^+ : CO_2^+$ ratio (green: AMS; red: SP-AMS), which was constant for the AMS (dashed line shows the result of a linear regression of CO^+ against CO_2^+). Shaded regions exemplify "starting" (green shading) and "flaming" (red shading) phases, defined using the $CO^+ : CO_2^+$ ratio.

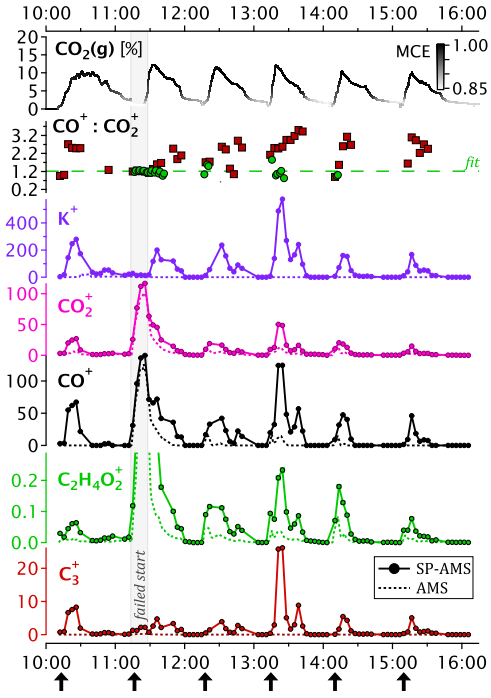

Figure 2. Time series for the aged beech-wood-combustion experiment. All traces are analogous to Fig. 1 but are scaled differently. Note especially the change of scale for $C_2H_4O_2^+$. In this experiment, the second batch of wood failed to start (grey shading), causing OM concentrations tenfold greater than normal. This especially increased the signal at $C_2H_4O_2^+$ (a tracer ion for holocellulose pyrolysis), which has been plotted off-scale during that period to allow features at other times to be visible. The MCE during this period was also off-scale, with mean 0.82.

in both AMS and SP-AMS. The proportion of this water signal originating from the thermal decomposition of OM was estimated in proportion to CO_2^+ by assuming a 1 : 1 $H_2O^+ : CO_2^+$ ratio, based on laboratory measurements of fulvic acid (Alfarra et al., 2004) and smog-chamber secondary OM (Kiendler-Scharr et al., 2009; Sun et al., 2010; Chen et al., 2011). However, the molecular composition of fresh wood-smoke aerosols is considerably different from such OM, containing an abundance of aldehydic, phenolic, and alcoholic functional groups from lignin, cellulose, and hemicellulose (Shafizadeh, 1984; Simoneit et al., 1993, 1999; Glassman and Yetter, 2008). This chemical composition and the high $CO^+ : CO_2^+$ ratio of the present sample (discussed below) suggest that this 1 : 1 ratio is likely to be biased low.

2.3.4 Potassium signals

SP-AMS and AMS signals are generally proportional to vaporized particulate mass due to the two-step vaporization/ionization process in the instrument. However, species with especially lower ionization potentials such as potassium may undergo one-step thermal ionization during the vaporization process (e.g., Drewnick et al., 2006). Due to this unique ionization mechanism, K^+ ions are normally observed with a unique distribution of kinetic energies, i.e., a uniquely broad peak shape in the mass spectrum. This means that the peak-integration routines programmed into PIKA are not applicable to K^+. Potassium-ion signals were therefore estimated as the total, baseline-subtracted signal at m/z 39 ± 0.2 minus the PIKA-fitted (Sect. 2.3) signal for the two ions which fell within that range, $C_3H_3^+$ and $^{13}CC_2H_2^+$. The closed background (Sect. 2.2) obtained in this way was subtracted from the analogous open signal. The unique behaviour of potassium ions in this study provides validation that all other ions, including those from BC, underwent two-step vaporization/ionization in the SP-AMS.

2.3.5 Particle collection efficiencies (CEs)

For SP-AMS and AMS signals to be quantified, the efficiency by which particles of different size, composition, and mor-

phology are vaporized must be known. This efficiency relies on (i) the transmission of particles from sample to vaporizer, and (ii) the successful vaporization of transmitted particles.

The geometry of the AMS and its thermal vaporizer has been designed such that point (i) above is negligible for particles of aerodynamic diameter between 60 and 600 nm (Huffman et al., 2005). For such particles, the CE of the AMS is governed by the probability of particle bounce at the thermal-vaporizer surface (e.g., Matthew et al., 2008; Middlebrook et al., 2012; Docherty et al., 2013). As discussed extensively in a separate publication (Corbin et al., 2015a), we evaluated the available literature on wood-combustion OM to arrive at a CE of 1.0 for both fresh and aged emissions.

Point (ii) above is negligible for BC-containing particles as the laser power is normally operated in a regime of excess power (Onasch et al., 2012). However, point (i) above is not negligible Willis et al. (2014), because the SP-AMS laser vaporizer is physically smaller than the AMS thermal vaporizer (with an estimated 40 % less effective area; Corbin et al., 2015c).

Thus, point (i) may lead to a negative SP-AMS bias if particles are too small to be adequately focussed into the SP-AMS laser beam. In this context, small refers to the aerodynamic size of the particles, which is a function of particle volume, morphology, and density. Willis et al. (2014) demonstrated that particle focussing is an issue for the SP-AMS for nebulized carbon-black particles of mobility diameter 200 nm. Although the aerodynamic diameter of those particles was not reported, this is a relatively large size when considering freshly formed soot (Sorensen, 2011), and so the effects observed by Willis et al. (2014) also apply to this study. Moreover, nebulized carbon black is likely to have a significantly smaller dynamic shape factor than the freshly formed fractal-like soot (Gysel et al., 2012) emitted by flames and combustion engines and likely emitted during the present experiments.

We thus expect that particle focussing lends a significant bias to the SP-AMS signals in this study, corresponding to a CE less than unity for the SP-AMS. However, the present particles were generally small relative to the lower limit of the SP-AMS aerodynamic lens (as discussed further for this data set in Corbin et al., 2015a), so that coating of these particles by secondary OM would likely change their ability to be focussed into the SP-AMS laser. In addition, particle morphology is expected to change significantly within burns (Leskinen et al., 2014). A single collection efficiency based on an external rBC mass reference, as has been applied in previous SP-AMS studies (Onasch et al., 2012; Massoli et al., 2012; Fortner et al., 2012; Cappa et al., 2014; Dallmann et al., 2014), would therefore not be possible. A time-resolved collection efficiency would require the assumption of internal mixing, and a reference instrument was in any case not available. Below, we focus instead on the changing SP-AMS signals and their relationship to AMS signals.

2.3.6 Relative ionization efficiencies (RIEs)

RIEs were applied to the SP-AMS and AMS data to represent variations in the instrumental sensitivity to different species (Jimenez et al., 2003). The RIE is the efficiency with which a given gas molecule is ionized relative to the AMS calibration standard, NO_3^- in ammonium nitrate.

The RIE(C_x^+) was set to 0.2 based on Onasch et al. (2012). This is likely an underestimate as it was derived without accounting for the SP-AMS CE (Willis et al., 2014) and because it did not account for refractory CO_x^+ species (rCO_x^+; Corbin et al., 2015c). However, in the absence of additional information on the SP-AMS CE (see above), we have used this RIE to provide an estimate of the relative intensity of C_x^+ signals in the mass spectra shown below.

The RIE(OM) was set to 1.4 based on Jimenez et al. (2003). This value was extrapolated to RIE(rCO_x^+) because both OM and rBC yield molecular CO and CO_2 upon thermal decomposition (Corbin et al., 2015c). Although the SP-AMS sensitivity to BC surface groups has not been established experimentally, it appears to be higher than that of C_x^+ based on the fact that the raw signals of rCO_x^+ were much higher than those of C_x^+ in this study. These high signals indicate that RIE(rCO_x^+) > RIE(C_x^+), since rBC is, by definition, composed primarily of graphitic carbon (Heidenreich et al., 1968; Bond et al., 2013; Petzold et al., 2013) and since rBC particles are completely vaporized in the SP-AMS (Onasch et al., 2012). In addition, the assumed RIE(rCO_x^+) of 1.4 implies an elemental composition of about 10 % oxygen in the BC, consistent with elemental analyses from the literature (Akhter et al., 1985b; Figueiredo et al., 1999). However, this value should be carefully validated before being used for mass quantification.

The SP-AMS and AMS RIE(K^+) are likely different given that potassium was thermally ionized and that the temperatures experienced by potassium in the SP-AMS and AMS vaporizers are different. For the AMS, an RIE(K^+) of 2.9 has been reported by Drewnick et al. (2006), while no data are available for the SP-AMS. To reflect a lack of information, RIE(K^+) was simply set to unity.

All other ions discussed below are considered organic and therefore assigned an RIE of 1.4 in PIKA. SP-AMS signals were not calibrated to mass in this study because the fraction of rBC focussed into the laser is dependent on soot-particle shape and coating (Onasch et al., 2012; Corbin et al., 2015c; Willis et al., 2014).

2.4 SP-AMS and AMS uncertainty analysis

2.4.1 Application of new positive matrix factorization (PMF) error model

Independent of peak-overlap uncertainties, peak integration in PIKA leads to a constant relative imprecision (fractional imprecision) which is expected to be approximately con-

stant for a given peak in a given data set (Corbin et al., 2015b). Peak-integration imprecisions arise from (i) peak-width-calibration imprecision and (ii) peak-fitting imprecisions that arise due to m/z-calibration biases (i.e., the finite mass accuracy of the instrument) and m/z-calibration imprecisions (Corbin et al., 2015b).

Although peak-fitting imprecisions may become much larger for overlapping peaks relative to isolated peaks (Corbin et al., 2015b; Cubison et al., 2014), peak overlap was not addressed quantitatively here (the final details of the method described by Corbin et al., 2015b, were not yet available). We have applied a simplified approach by assuming an approximately constant value of $\sim 4\,\%$ for (ii) above, which was estimated from the Monte-Carlo-estimated fitting imprecision for isolated peaks in the present data set (Corbin et al., 2015b).

For (i) above, we used the measured imprecision of in our peak-width calibration of 2.5 % (Corbin et al., 2015b). The quadratic sum of these fractional uncertainties, 4.7 %, gave the peak-integration uncertainty, as described in Corbin et al. (2015b).

This percentage peak-integration uncertainties were combined in quadrature with a Poisson uncertainty term to yield an uncertainty model which is dominated by ion-counting uncertainty for low signals and by peak-integration uncertainties for high signals (for this data set, those greater than ~ 1000 counts per second for a given peak; Corbin et al., 2015b).

2.4.2 Additional uncertainties

In addition to the error model discussed above, additional uncertainties were assigned to CO^+, CHO^+, CHO_2^+, and $C_3H_3^+$, for various physical reasons, as shown in Table 1. These additional uncertainties were only calculated for ions which were of significant signal in the mass spectrum. Table 1 also shows the default uncertainties for above-detection-limit (Corbin et al., 2015b) and below-detection-limit (Ulbrich et al., 2009) signals.

The increased CO^+ detection limit accounts for the failure of the PIKA peak-integration algorithm to integrate peaks below a ~ 1 kHz "detection limit" caused by the neighbouring N_2^+ signal. This behaviour is expected for peaks with a very small intensity relative to an overlapping peak (Corbin et al., 2015b). The validity of CO^+ above this DL was confirmed by their linear variation with CO_2^+ in the AMS, with slopes fully consistent with the literature as detailed elsewhere (Corbin et al., 2015a). To address this detection limit, backgrounds were subtracted prior to fitting ("Diff" mode in PIKA) for CO^+, reversing the normal procedure (i.e., "OminusC" mode in PIKA). An uncertainty of $3.5 \times$ DL was assigned to below-DL values according to common practice in the PMF community (Polissar et al., 1998; Hopke, 2000; Reff et al., 2007), although the results were not sensitive to the chosen value. Below-DL values were not replaced since this was not a detection limit in the conventional sense. The additional uncertainty in CO^+ signals due to their overlapping with N_2^+ (Cubison et al., 2014; Corbin et al., 2015b) was not modelled.

The uncertainty in CHO^+ (m/z 29) was increased to reflect the fact that the signal intensity of $^{15}NN^+$ (m/z 29) was constrained by the signal intensity at N_2^+ (m/z 28) in PIKA using a relative abundance of ^{15}N predicted according to de Laeter et al. (2003) (Sueper et al., 2011). In contrast to the majority of isotopically constrained fits, the actual uncertainty of the signal assigned to $^{15}NN^+$ was therefore very large relative to the initially estimated CHO^+ uncertainty. To account for this, $\sigma\left(^{15}NN^+\right)$ was added in quadrature to the original uncertainty in CHO^+ (Table 1). This procedure provides only a rough estimate of the true uncertainty, as it assumes that the uncertainty $\sigma\left(CHO^+\right)$ is independent of the constrained-fit procedure, which is generally not true (Cubison et al., 2014; Corbin et al., 2015b).

The uncertainty in CHO_2^+ suffered from a constrained $^{13}CO_2^+$ fit, similarly to the case of CHO^+ and $^{15}NN^+$, and was treated similarly.

The final ion in Table 1, $C_3H_3^+$, was overestimated in the presence of high SP-AMS K^+ signals. This overestimation was made apparent by examining background mass spectra (chopper blocking the particle beam), in which K^+ signals were negligible but $C_3H_3^+$ signals remained. These background spectra were used to estimate a $C_3H_3^+$ overestimation of $\sim 2\,\mu g\,m^{-3}$ when K^+ was highest. This simple estimate was represented numerically as $1 \pm 3\,\mu g\,m^{-3}$, scaled by the time series of SP-AMS K^+, and subtracted from the SP-AMS $C_3H_3^+$ signals. The corresponding uncertainty was estimated according to this subtraction, which is considered a reasonable estimate since the influence of the K^+ background on the peak shape appeared to be negligible, by inspection. No $^{41}K^+$ interference was observed so no changes were made at m/z 41. Similarly, AMS potassium signals (i.e., when the SP laser was off) were too low for interference from K^+ to be an issue.

2.5 Positive matrix factorization

PMF assumes that a matrix of data can be explained by a linear combination of factors with characteristic profiles and varying temporal contributions (Paatero and Tapper, 1994; Ulbrich et al., 2009). The PMF model has been widely and successfully applied to AMS data (Lanz et al., 2007; Ulbrich et al., 2009; Zhang et al., 2011). Applying PMF to AMS or SP-AMS data entails the assumption that the overall mass spectrum can be described by a small number of characteristic mass spectra (Lanz et al., 2007; Ulbrich et al., 2009; Zhang et al., 2011), which is evaluated during PMF analysis by inspection of the model residuals (Paatero and Tapper, 1994; Paatero et al., 2002; Ulbrich et al., 2009; Zhang et al., 2011).

Table 1. AMS and SP-AMS uncertainties σ used in this study and their detection limits (DLs). $I\left(X^+\right)$ is the rate of counts of ion X^+; $\hat{I}\left(X^+\right)$ is $I\left(X^+\right)$ normalized to its maximum value; $R\left(X^+\right)$ is the abundance of an ion X^+ relative to its most abundant isotopologue; and k is a constant determined as $1\,\mu g\,m^{-3}$ as discussed in the text.

Species	Signal	Uncertainty	Rationale
Default	I	$\sigma = \sqrt{\sigma_{\text{counting}}^2 + \sigma_A^2}$ if >DL $\sigma = \sigma_{\text{counting}}(1)$ if <DL of 1 ion.	Combined poisson and peak-integration uncertainties (Corbin et al., 2015b).
CO^+	I	$\sigma\left(CO^+\right)$ if >DL, 3.5 × DL if <DL of 1 kHz.	Higher-than-normal DL due to poor resolution from N_2^+.
CHO^+	I	$\sqrt{\left[\sigma\left(CHO^+\right)\right]^2 + \left[R\left(^{15}NN^+\right)\right]^2}$	Fit to the overlapping $^{15}NN^+$ peak constrained by N_2^+.
CHO_2^+	I	$\sqrt{\left[\sigma\left(CHO_2^+\right)\right]^2 + \left[R\left(^{13}CO_2^+\right)\right]^2}$	Fit to the overlapping $^{13}CO_2^+$ peak constrained by CO_2^+.
$C_3H_3^+$	$I\left(C_3H_3^+\right) - k \times \hat{I}(K^+)$	$\sqrt{\left[\sigma\left(C_3H_3^+\right)\right]^2 + \left[3k \times \hat{I}\left(K^+\right)\right]^2}$	Interference by tailing of extremely high SP-AMS K^+ signals from rBC.

PMF analysis was conducted using the PMF Evaluation Tool (Ulbrich et al., 2009; Zhang et al., 2011). Before analysis, signals were integrated and exported using the peak-integration approach and new uncertainty model described in the Supplement and in Sect. 2.4. Ash signals, defined as ions containing Cl, Si, K, or other metals, were excluded from the model. The number of PMF factors used, P, was chosen based on the degree to which the model improved with increased P, as evaluated by the structure of model residuals in temporal and m/z space. In general, increasing P beyond the values presented herein only served to better explain spikes in OM concentration at the start of each burn. Therefore, the conclusions discussed below are insensitive to the chosen P.

The large number of zeroes in this data set meant that ambiguity due to possible linear transformations of the PMF solution ("rotational ambiguity") was negligible in this data set (Paatero and Tapper, 1994; Paatero et al., 2002). Similarly, there was no evidence for local minima (see Supplement).

The large range of signals observed in the present study led PMF to report "unique factors" (Paatero and Tapper, 1994) containing a single ion such as CO^+ when using the old uncertainty model. This was corrected by the Corbin et al. (2015b) uncertainty model (Sect. 2.4), which provides a more even weighting for high and low signals. We note that the linear uncertainty term in the Corbin et al. (2015b) model is similar to the ad hoc "C3" parameter of PMF (Paatero, 2000, labelled "model error" in PET). The difference is that the value of the linear uncertainty term was estimated from the data, and that it was added in quadrature rather than linearly to the pre-existing Poisson uncertainties, since its physical origin is independent of counting uncertainties (Corbin et al., 2015b).

The new uncertainty model also generally reduced signal-to-noise ratios (SNRs) such that previous outliers (in weighted-residual space) from major ions such as CO^+ and C_3^+ became more comparable to other species. Corbin et al. (2015b) show that such outliers may arise purely from the omission of a linear uncertainty term when such an uncertainty exists. The outliers therefore do not indicate measurement errors, peak-integration errors, or transient signals. The new uncertainty model also increased the number of "weak" variables, defined as having SNR below 2 (Paatero and Hopke, 2003; Ulbrich et al., 2009), which were down-weighted by a factor of 2. No variables were "bad" in the sense of having SNR < 0.2 (Paatero and Hopke, 2003). Additional details on the PMF analysis, including residual plots, are available in the Supplement.

3 Results

3.1 Temporal evolution of burns

Figures 1 and 2 illustrate the temporal evolution of the fresh and aged emissions using selected SP-AMS and AMS marker ions. Also shown in the figure is the pre-dilution CO_2(g) concentration, which is proportional to the combustion rate. The CO_2(g) also indicates the airflow into the chimney, which implicitly dilutes the emissions to a varying degree. Following the addition of a batch of wood (black arrows along the abscissa), CO_2(g) increases rapidly ("starting phase") before reaching a relatively stable level ("flaming phase") and finally dying off ("smouldering phase" with negligible emissions).

During the starting phase, the wood was only partially aflame, typically in only one region. Both fresh (Fig. 5) and aged (Fig. 6) OM emissions were highest during this phase.

The degree of oxidation and emission factors of this OM has been reported in detail elsewhere (Corbin et al., 2015a).

The starting-phase OM emissions are illustrated by the $C_2H_4O_2^+$ signal in Fig. 1. This ion is correlated with cellulose/hemicellulose pyrolysis products such as levoglucosan and other anhydrosugars (Lee et al., 2010) and its signal spiked when each batch of wood was added (black arrows on the abscissa) and died away thereafter. Similar trends were seen for the oxidized emissions (Fig. 2), although the $C_2H_4O_2^+$ signal was much lower in that case. The SP-AMS and $C_2H_4O_2^+$ signals were not always well correlated, as discussed in Sect. 4.3.

The starting phase ended once flames had completely engulfed the wood. In this "flaming phase" most volatilized organics were destroyed in the flames such that emissions were comprised of little OM but significant amounts of refractory black carbon. This is illustrated in Figs. 1 and 2 by the C_3^+ ion, which in the SP-AMS represents rBC (Onasch et al., 2012; Corbin et al., 2015c).

Black carbon was not the only SP-AMS species observed during the flaming phase. Signals from two other species, K^+ and CO_x^+ ($= CO^+ + CO_2^+$), remained extremely high during this phase (Figs. 1 and 2). These signals dropped to negligible levels in the AMS (dashed lines in Fig. 1), confirming that they were generated from LR-PM particles. Although high K^+ signals were only observed in the SP-AMS, relatively high CO_x^+ signals were observed in both AMS and SP-AMS. These signals therefore appear to have originated from both OM and rBC.

The $CO^+ : CO_2^+$ ratio for these signals provided a useful metric of comparison between SP-AMS and AMS across burn periods. In the AMS, this ratio was 3.92 ± 0.01 for fresh emissions but 1.22 ± 0.01 for aged emissions (Corbin et al., 2015a). This latter ratio is in good agreement with observations of atmospherically oxidized OM (0.9–1.25, Aiken et al., 2008), indicating a relative increase of CO_2^+ due to the thermal degradation of oxidation-formed carboxylic acids or peroxides on the AMS vaporizer (Ng et al., 2011). In contrast, the phenols, alcohols, and aldehydes that are abundant in fresh wood (Shafizadeh, 1984; Simoneit et al., 1993, 1999) are more likely to yield CO^+ than CO_2^+ when vaporized, giving the high $CO^+ : CO_2^+$ ratio of 3.92.

The SP-AMS $CO^+ : CO_2^+$ ratio was not different from the AMS ratio during the starting phases (Figs. 1 and 2) nor during the filtered and oxidized experiment (not shown). This suggests that OM fragmentation in the SP-AMS and AMS was comparable, at least in terms of CO_x^+ fragments.

In contrast to the OM-dominated starting phase, the SP-AMS $CO^+ : CO_2^+$ ratio increased significantly during the flaming phase, increasing from ~ 4 to ~ 6 for the fresh case and from ~ 1 to ~ 2 for the oxidized case.

3.2 SP-AMS and AMS mass spectra

3.2.1 Fresh emissions

Figure 3 shows SP-AMS and AMS carbonaceous-ion mass spectra for the starting- and flaming-phase periods of the fresh-emissions experiment that are highlighted in Fig. 1. Ions are coloured according to their oxygen content, and signals at integer m/z are stacked for clarity. Ash species such as K^+ (the most intense ion), Cl^+, HCl^+, Zn^+, SO^+, and SiO_2^+ (all low intensity) were excluded since these species are not susceptible to oxidation in the MSC.

The SP-AMS and AMS mass spectra in Fig. 3a and 3b are similar during the starting phase when OM was highest. This explains why the SP-AMS $CO^+ : CO_2^+$ ratios in Figs. 1 and 2 are similar to the AMS ratios.

In contrast to the starting phase, Fig. 3c and d show that the flaming-phase PM consisted mostly of refractory PM. The AMS signals during this phase were negligible. (Note that the ordinate maximum of Fig. 3d is 2 orders of magnitude smaller than Fig. 3c.) Thus the SP-AMS mass spectrum shows that the rBC particles yielded C_x^+ and CO_x^+ (and K^+) from refractory species.

The other major signals in the flaming-phase SP-AMS mass spectrum are the carbon-cluster ions C_x^+ with $1 \leq \times \leq 3$. Another study by our group (Corbin et al., 2015c) found that the ratios between these ions was indicative of the underlying structure of the rBC, with rBC particles that generated fullerenic ions having $C_1^+ : C_3^+$ ratios close to and other samples having $C_1^+ : C_3^+$ ratios below 0.8. The $C_1^+ : C_3^+$ ratio observed in Fig. 3c, where AMS signals are negligible, is close to unity. This is an exception to the trends observed by Corbin et al. (2015c) and others (Onasch et al., 2012; Canagaratna et al., 2015). In contrast, the more robust but lower-sensitivity ratio $C_4^+ : C_3^+$ was well within the 0.01–0.07 range reported by Corbin et al. (2015c), for both fresh and aged emissions. The $C_4^+ : C_3^+$ ratio and not the $C_1^+ : C_3^+$ should therefore be used in source apportionment studies.

3.2.2 Aged emissions

Figure 4 shows mass spectra from the third burn of the aged-emissions experiment. The overall trends between SP-AMS and AMS are similar to those discussed in the previous subsection. However, both SP-AMS and AMS starting-phase mass spectra (Fig. 4a and b, respectively) show relatively lower signals from hydrocarbon fragments (green bars) and relatively higher signals from CO_x^+ ions due to oxidative functionalization of the OM.

Similarly to the fresh-emissions case, flaming-phase CO_x^+ signals were of comparable magnitude to C_x^+ signals in the SP-AMS (Fig. 4c). However, CO_2^+ increased relative to both C_3^+ and CO^+, indicating oxidation of the species which generated CO_x^+. We note that surface oxidation is not expected to significantly influence SP-AMS C_x^+ signals, since these

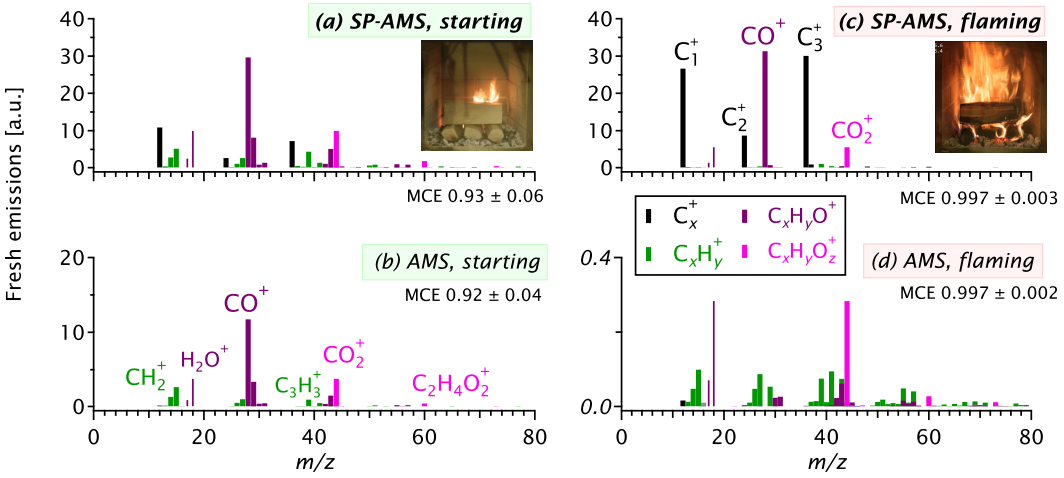

Figure 3. Fresh-emissions SP-AMS and AMS mass spectra for the starting-phase (highest OM emissions) and flaming-phase (lowest OM emissions, high BC emissions, Fig. 1) beech-combustion experiments. All signals have been scaled by representative RIEs. The estimated signals at O^+, OH^+, and H_2O^+ have been estimated from CO_2^+ (Sect. 2.3) and therefore plotted with thinner bars. The insets show photographs of a typical burn. The mean and standard deviation of the MCE over the averaged period of time is included. Note the changes of scale in panels **(c)** and **(d)**. In panel **(d)**, no CO^+ signal is shown as that species was below its detection limit (2.4 units).

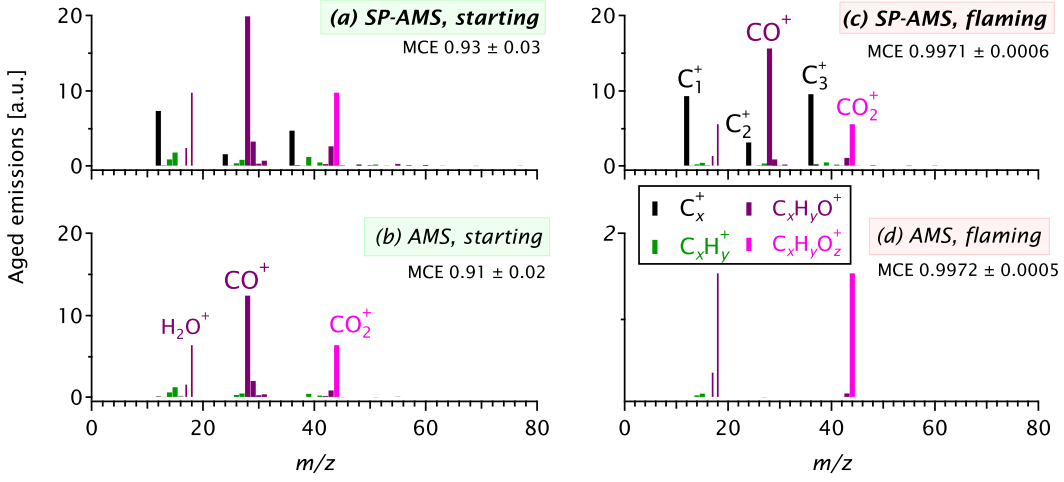

Figure 4. Aged-emissions SP-AMS and AMS mass spectra for the starting-phase (highest OM emissions) and flaming-phase (lowest OM emissions, high BC emissions) beech-combustion experiments, in analogy to Fig. 3. Note the change of scale in panel **(d)**. The estimated signals at O^+, OH^+, and H_2O^+ have been estimated from CO_2^+ (Sect. 2.3) and therefore plotted with thinner bars. In panel **(d)**, no CO^+ signal is shown as that species was below its detection limit (2.4 units).

signals represent the bulk composition of the solid rBC. The chemical species generating C_x^+ and CO_x^+ signals remained largely refractory after oxidation as indicated by the AMS data, which are plotted in Fig. 4d with an order-of-magnitude-smaller ordinate maximum.

3.3 Positive matrix factorization

The discussion in Sect. 3 highlighted selected ions and mass spectra from selected time periods in the burn cycle. To generalize this discussion to the entire mass spectrum and the entire burn cycle, PMF was performed on the fresh and aged data. The utility of PMF was to reduce 399 measured ions in over 100 mass spectra to 3–4 "factors" with mass spectra and time series describing > 92 % of the variance in the data. (Over 97 % of the variance would have been explained had the failed-start burn been excluded.) These PMF factors are discussed below.

3.3.1 Fresh emissions

With the exception of BC factors, each fresh SP-AMS PMF factor had an analogous factor in the AMS data. This is shown in Fig. 5a–c. Each panel in the figure shows the

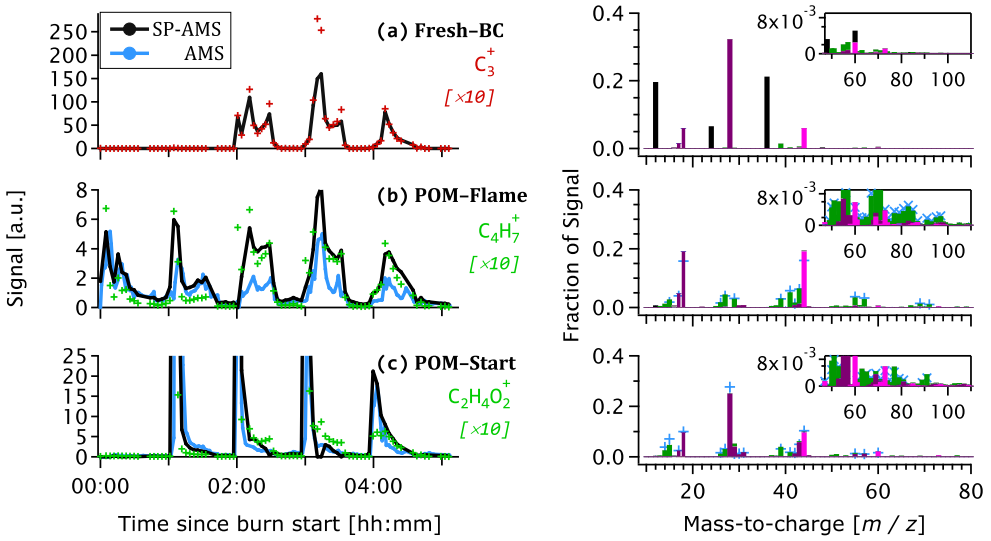

Figure 5. PMF factors for fresh-emissions data. The left column shows SP-AMS factor time series (black) together with AMS time series (blue) and selected SP-AMS tracer ions (symbols). The right column and insets shows the corresponding SP-AMS factor mass spectra using the same colour scheme as Fig. 3: black ions are carbon clusters, green ions are hydrocarbon fragments, and pink/purple are more- or less-oxygenated carbon-containing ions. The right-column blue symbols show the AMS mass spectra for data >1 % (or >0.1 %) of the spectrum in the main panel (or inset). Signals for **(c)** POM–Start are drawn off-scale to show key structural features. In the mass spectra of **(b)**, no CO^+ signal is shown as that species was below its detection limit (see text).

time series for each PMF factor in black (SP-AMS) or blue (AMS). The smoothness of each factor time series should not be compared because only half as many SP-AMS data were available as for the AMS (Sect. 2.2). The time series in Fig. 5 also include arbitrarily scaled raw signals of selected ions.

Figure 5a shows the first PMF factor, "Fresh–BC", with a mass spectrum similar to the SP-AMS flaming-phase mass spectrum (Fig. 3). The mass spectrum is plotted following the scheme introduced in Fig. 3. The time series of this factor closely followed that of C_3^+ except during spikes in concentration. These exceptions may reflect a change in instrument response, for example due to detector saturation. Alternatively, they may reflect a change in PM composition, for example due to the wood logs shifting position during combustion (cf. Fig. 1a, inset) and causing a transient change in rBC composition.

The observation of both CO_x^+ and C_x^+ signals in the Fresh–BC factor suggests that the two species originated from the same physical source (see also Fig. 1). To test whether the CO_x^+ might have been attributed to a separate factor from C_x^+ with more PMF factors, we increased the number of PMF factors as high as 10. The result was two separate C_x^+-containing factors, both of which remained associated with CO_x^+ in a similar manner to Fresh–BC. This suggests that these two species were physically related, possibly originating from a single process in the combustion.

The next factor in the figure is "POM–Flame" (Fig. 5b). This primary OM factor is named for its sustained signal during the flaming phase discussed above, though it is important to note that the other OM factor ("POM–Start") was simultaneously present at comparable intensity.

POM–Flame was better correlated with the alkyl ion $C_4H_7^+$ (Fig. 5b) than with the pyrolysis tracer $C_2H_4O_4^+$. The SP-AMS mass spectrum for this factor is shown in Fig. 5b. An analogous AMS factor, with similar temporal trend and mass spectrum, was also identified and is included in the figure. The AMS mass spectrum is included as the summed signal at integer m/z since one ion typically dominated this sum, as shown by the coloured SP-AMS signals. For simplicity, AMS data are only shown for signals contributing >1 % (or >0.1 %) of the total in the main panel (or inset) mass spectrum.

The AMS and SP-AMS POM–Flame mass spectra were virtually identical. Both showed considerable amounts of large hydrocarbon fragments (Fig. 5b, inset). Neither POM–Flame spectra included CO^+ because the low concentrations of POM–Flame meant that this ion was below its detection limit.

The final factor in Fig. 5, POM–Start, contributed more to overall OM signals than POM–Flame and made most of its contribution during the starting phase of each burn (Fig. 5c).

POM–Start was absent for the first burn, along with the anhydrosugar tracer $C_2H_4O_4^+$. This is most likely because in the first burn combustion was initiated by tinder placed atop the wood, whereas in subsequent burns combustion was initiated from below by the hot embers of the previous burn (Sect. 2). Using $C_2H_4O_4^+$ as a wood-combustion tracer in

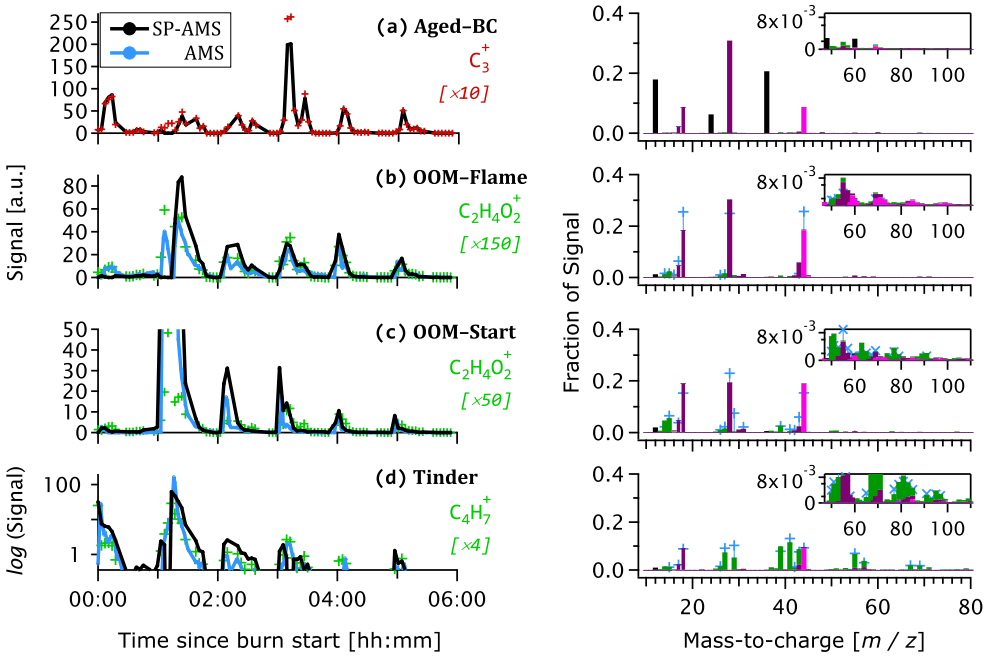

Figure 6. PMF factors for aged-emissions data. Panels are analogous to Fig. 5. Signals for **(c)** OOM–Start are drawn off-scale to show key structural features. Time series **(d)** is plotted on a log-scale due to its low intensity, with an axis minimum of the OM limit of detection (3σ). In the mass spectra of **(d)**, no CO^+ signal is shown as that species was below its detection limit (see text).

an atmospheric context may therefore underestimate wood-combustion emissions in some cases.

3.3.2 Aged emissions

The aged-emissions PMF factors could be viewed as analogous to the fresh-emissions results. The lesser signals at higher m/z were reduced in each analogous aged mass spectrum, as expected since highly oxidized species fragment during vaporization/ionization to a much greater extent than reduced ones (Canagaratna et al., 2007).

An Aged–BC factor was well correlated with C_3^+ (Fig. 6a). The Aged–BC mass spectrum was dominated by the same C_x^+ and CO_x^+ ions as the Fresh–BC but in different relative intensities. The ratio $C_3^+ : CO_2^+$ decreased from 3.5 to 2.4 after aging, while the ratio $CO^+ : CO_2^+$ decreased from 5.4 to 3.5. The source of CO_x^+ therefore both increased and became more oxidized following aging. The absence of an analogous AMS factor suggested that the source of this BC-associated CO_x^+ remained refractory after aging.

An OOM–Flame (oxidized OM, flaming phase) factor analogous to POM–Flame was also observed. Figure 6b shows that this factor was well correlated with $C_2H_4O_2^+$. Here, the $C_2H_4O_2^+$ tracer is much lower in intensity than for the fresh-emissions case (cf. Figs. 1 and 2) due to its susceptibility to oxidative aging (Hennigan et al., 2010; Knopf et al., 2011; Slade and Knopf, 2013). However, this reduction in $C_2H_4O_2^+$ intensity does not invalidate its use as a pyrolysis tracer. The more-common oxidized-OM tracer, CO_2^+ (Zhang et al., 2005; Grieshop et al., 2009; Jimenez et al., 2009; Donahue et al., 2012), was inappropriate in this case due to its confounding refractory source in Aged–BC. The resulting ambiguity in the interpretation of CO_2^+ in BC-rich aerosols is likely to be significant in atmospheric SP-AMS studies.

The OOM–Start factor corresponded to higher OM loadings than, and followed similar trends to, POM–Start. This factor was present at extremely high loadings during the failed-start case (off-scale in Fig. 6c; re-plotted in Fig. S2 in the Supplement). Its signals at higher m/z (Fig. 6c, inset) were relatively higher than for OOM–Flame, possibly because oxidation in the MSC was less extensive when organic vapour concentrations were higher.

The fourth aged-emissions factor was the tinder factor, corresponding to the paraffin-soaked wood shavings used to start the fire (Sect. 2) and to re-ignite the failed-start burn (Fig. 6d, $\sim 01:10$). (Prior to this re-ignition, the air flow into the stove was changed and the door was afterwards opened briefly.) The tinder mass spectrum was dominated by hydrocarbon fragments $C_xH_y^+$. It also contained some CO_2^+ (and probably below-detection-limit CO^+) due to oxidation in the MSC.

Note that tinder was also used at the beginning of the fresh-emissions experiment, and an analogous PMF factor did initially result for that experiment. However, only the first two measurements of the fresh-emissions experiment were strongly impacted by this contaminant. To simplify the PMF

model needed to describe the data, the first two measurements of that experiment were downweighted threefold (see Supplement) for the fresh emissions.

4 Discussion

The measurements presented above provide evidence for the presence and oxidative enhancement of refractory rBC surface groups and for a pyrolytic origin of the OM in beech-wood soot. These and other compositional features of the soot are discussed below. A detailed discussion of the oxidized OM can be found elsewhere (Corbin et al., 2015a).

4.1 rCO_x^+ from BC surface groups

The combination of non-refractory AMS and refractory SP-AMS measurements of CO^+ and CO_2^+ (Figs. 3c–d and 4c–d) clearly showed that the majority of these signals originated from refractory species (rCO_x^+). These refractory CO_2^+ signals became more intense after oxidative aging, indicating that they originated from incompletely oxidized species. The change in the ratio of the rCO_x^+ signals after aging indicated a change in the chemical species producing these signals.

These two observations reduce the likelihood of confounding sources of rCO_x^+ generating the majority of the signal. Carbonates such as $CaCO_3$ (Westberg et al., 2003) cannot be oxidized as observed. Refractory organics such as large, oxidized polyaromatic hydrocarbons may generate CO_x^+ but would also produce other, hydrogen-containing, ions in the mass spectrum. Additionally, if the refractory organics had not contained hydrogen, the observed increase in CO_x^+ after aging would be impossible.

This increase in CO_x^+ is consistent with soot formation mechanisms: soot only forms in oxygen-deprived environments (Frenklach, 2002) and initially condenses as PAH-like nanoparticles before graphitizing via loss of hydrogen (Dobbins, 2002; D'Anna, 2009). Oxygen is normally gained during later oxidation, before exiting the flame, for example by flame-produced radicals like $OH^\bullet$ (Tree and Svensson, 2007; Glassman and Yetter, 2008).

Since well over 90 % of soot produced in a flame is destroyed the abovementioned in-flame oxidation, all soot is expected to contain oxygenated surface groups (Akhter et al., 1985b; Mul et al., 1998; Figueiredo et al., 1999; Hopkins et al., 2007; Vernooij et al., 2009). The BC surface functional groups are observed as CO_x^+ and not, say, C_3CO^+ because BC surface groups thermally decompose at much lower temperatures than the vaporization temperature of BC (Corbin et al., 2015c).

We cannot completely rule out the role of adsorbed CO(g) or CO_2(g) in forming rCO_x^+. This is an inherent weakness of the destructive SP-AMS technique relative to FTIR and NEXAFS. However, the significant change in CO_x^+ upon oxidation indicates that such a role was not dominant. Additionally, if the thermal stability of covalently bonded or adsorbed species at the BC is similar, reaction mechanisms (Smith and Chughtai, 1997; Monge et al., 2010) may be also be similar in both cases.

4.2 Atmospheric implications of BC surface groups

Two atmospherically relevant observations can be made regarding BC surface groups. First, the PMF results show that the relative amount of these surface groups can be regarded as constant throughout the burn. Regardless of burn stage, stove temperature (cf. first burn in Fig. 6), or the concentration of emitted BC, a single PMF factor adequately represented these signals. It may therefore be possible to model the surface of beech-wood BC as a single chemical species. This single chemical species is likely to undergo complex chemistry given that laboratory-generated alkane soot samples display different regimes of reactivity and are sensitive to photochemistry (Smith and Chughtai, 1997; Monge et al., 2010). Soot surrogates such as the *n*-hexane soot recommended by the International Steering Committee on Black Carbon Reference Materials (Schmidl et al., 2003) may therefore not provide an accurate representation of wood-combustion soot.

Second, the raw data, supported by PMF, show that the BC surface functionality changed considerably after aging. This is demonstrated by the change of $CO^+ : CO_2^+$ ratio after aging. Based on the PMF factors, this ratio decreased from 5.4 to 3.5 (a 54 % decrease). As mentioned above, these rCO_x^+ signals originate from the thermally driven desorption of different functional groups on the BC surface as CO(g) or CO_2(g) (Corbin et al., 2015c). Whether CO(g) or CO_2(g) desorbs is governed by the nature of the functional groups themselves. The mass of desorbed gases can be directly related to the mass of the initial functional groups (Figueiredo et al., 1999, 2007). Although the exact path of decomposition is sensitive to the heating rate (Zielke, 1996), the decrease of the $CO^+ : CO_2^+$ ratio after aging indicates an increased average oxidation of the BC surface groups. For example, the decreased ratio may have corresponded to the oxidation of phenolic or carbonyl groups at the BC surface (Figueiredo et al., 1999). In addition to the increased average oxidation of the BC surface upon aging, the absolute quantity of BC surface groups changed. This can be considered in terms of the $C_3^+ : CO_2^+$ ratio, which decreased from 3.5 to 2.4 (a 46 % decrease). This corresponds to an increase in the amount of functionalized carbon and indicates that the BC surface became more oxidized upon exposure to $OH^\bullet$ and O_3. However, the data cannot be used to estimate the absolute oxygen content of the BC until the SP-AMS sensitivity to rCO_x^+ is established by future studies (Sect. 2.2).

Our data represent the first time-resolved measurements of in situ BC surface aging. The SP-AMS may therefore be useful in the online measurement of BC surface groups in atmospheric studies. This would allow the competition between

BC oxidation and organic oxidation to be investigated, although oxidant concentrations in this study were higher than would be expected in the atmosphere (Sect. 2).

The majority of BC emissions always occurred in the flaming phase, during which organic concentrations were at their lowest in both the particle phase (Figs. 5 and 6) and the gas phase (Corbin et al., 2015a). This is because on the one hand large amounts of organic vapours are yielded by pyrolysis (Sect. 4.3) at temperatures lower than the ignition point of the fire, while on the other hand ignition triggers the flaming combustion which simultaneously generates soot and converts the emitted organics to CO(g) and CO_2(g) (Glassman and Yetter, 2008). The organic vapours which are emitted by flaming-phase combustion appear may have followed trajectories that avoid the flames, given that their mass spectra resemble the aliphatic products of lignin pyrolysis (4.3).

Given that most BC is emitted when little organics are emitted, and that BC was overall the major species emitted by this fire (Corbin et al., 2015a), the BC surface may represent a significant oxidant sink during the initial aging of a similar combustion plume. The actual significance of the BC in this case would depend on the degree of mixing between starting and flaming phases after emission and on the fate of co-emitted nitrogen and sulfur oxides.

It might be hypothesized that a functionalized BC particle would become more hygroscopic and therefore more likely to act as a CCN or ice nucleus. However, while our measurements are the first to directly observe the BC functionalizations in a wood-combustion aerosol, they do not directly affect the observations of previous studies on beech-wood soot which suggest a minor role in this regard (Martin et al., 2012; Chou et al., 2013). In the case of CCN, these and other studies (Kuwata et al., 2009) have indicated that mixing of beech-combustion soot with other aerosols via condensation or coagulation is the most likely pathway for their becoming CCN active.

In general, our conclusions apply only to a well-operated stove and, moreover, only to wood stoves. Under different operating conditions, stove emissions may change considerably (Elsasser et al., 2013; Eriksson et al., 2014). Less-efficient combustion systems such as open burning may produce more primary as well as secondary OM (Hennigan et al., 2011; Ortega et al., 2013). These higher organic emissions lead to a greater role of secondary OM in the evolution of particle hygroscopicity, which is also strongly dependent on the fuel (Engelhart et al., 2012).

4.3 Pyrolysis-formed OM

In general, the SP-AMS and AMS mass spectra were highly similar. Excluding C_x^+, the uncentred correlation coefficients (r_{UC}) between the two POM–Start and POM–Flame mass spectra were 0.99 and 0.93, respectively. Excluding all ions below m/z 44 (to account for refractory CO_x^+ signals and to reduce the influence of the highest signals) increased this r_{UC} to 0.993 and 0.997 for POM–Start and POM–Flame, respectively.

The mass spectrum of POM–Start was similar to that of pure levoglucosan (Aiken et al., 2007; Ulbrich et al., 2009, 2014), as shown in Table 2. This is consistent with the fact that $C_2H_4O_2^+$ signals (m/z 60), commonly used as a tracer for biomass-burning pyrolysis products like levoglucosan (Lee et al., 2010; Aiken et al., 2010; Hennigan et al., 2010, 2011; Cubison et al., 2011), were almost entirely explained by POM–Start in the PMF model. POM–Start is thus interpreted as reflecting wood pyrolysis, in particular the pyrolysis of cellulose, hemicellulose, and other carbohydrates ("holocellulose"). Holocellulose pyrolysis produces levoglucosan and other anhydrosugars (Shafizadeh, 1984; Simoneit et al., 1999) and occurs at appreciably lower temperatures than pyrolysis of the other major polymer in wood, lignin (Timell, 1967; Shafizadeh, 1984; Yang et al., 2007; Di Blasi, 2008). This thermal instability, together with the fact that holocellulose comprises about 70 % of beech wood (Timell, 1967), explains why POM–Start was the more-abundant POM factor. The high CO^+ signals associated with POM–Start (Fig. 5c) may therefore be explained as originating from the polyalcoholic sugars such as glucose and xylose which comprise holocellulose. The relatively low signal of CO_2^+ from POM–Start may be related to decarboxylation reactions within the stove during pyrolysis (Shafizadeh, 1984), similarly to the decarboxylation which produces CO_2^+ within the AMS and SP-AMS during vaporization (Duplissy et al., 2011).

An interesting feature of the POM–Start mass spectrum was the presence of aromatic ions such as $C_6H_5^+$ (phenyl) and $C_7H_7^+$ (benzyl). The fact that these ions originated from aromatic molecules was confirmed by their persistence in the OOM–Start mass spectrum due to the unusual stability of oxygenated aromatic molecules against fragmentation upon electron impact (McLafferty and Tureček, 1993). These aromatics may have formed during pyrolysis (Simoneit et al., 1993, 1999) or from the flame itself (Frenklach, 2002; Wang, 2011). Higher starting-phase signals of aromatics, including PAHs, have been observed by previous studies (Elsasser et al., 2013; Eriksson et al., 2014).

Since POM–Start was ascribed to holocellulose pyrolysis, it was hypothesized that POM–Flame may have been more closely associated with lignin pyrolysis, which generally requires higher temperatures (Shafizadeh, 1984). The alkyl fragments $C_nH_{2n-1}^+$ and $C_nH_{2n+1}^+$ seen in the POM–Flame mass spectrum (Fig. 5b) may be related to the cyclic aliphatic molecules, phytosterols, emitted together with substituted phenols during lignin pyrolysis (Genuit et al., 1987; Simoneit et al., 1993; Rogge et al., 1998).

The uncentred correlation coefficient between the mass spectra of pure burnt lignin (Ulbrich et al., 2009, 2014) and POM–Flame for the SP-AMS and AMS was relatively high (Table 2), suggesting that this association was reasonable.

However, the POM–Flame mass spectra were also well correlated with levoglucosan (Table 2), suggesting that either POM–Flame was not clearly separated from POM–Start during factor analysis or that POM–Start contained contributions from both lignin and holocellulose. Both are likely to be true to some degree (the factor separation issue is further discussed in the Supplement). In particular, although holocellulose pyrolyzes at lower temperatures, both holocellulose and lignin pyrolyze across a range of overlapping temperatures (Shafizadeh, 1984; Yang et al., 2007; Di Blasi, 2008), which would have led to a range of mass spectra being observed. Moreover, ash species such as potassium catalyze the pyrolysis process (Di Blasi, 2008), so the pure-lignin mass spectrum used here is not an ideal reference.

A second, distinct hypothesis for the origin of POM–Flame is the in-flame synthesis of aliphatic functionalities, as has recently been observed by Cain et al. (2010, 2011). This hypothesis is considered unlikely given the degree of oxygenation of POM–Flame.

4.4 Comparison of AMS and SP-AMS OM signals

The interpretation of the POM mass spectra as dominated by pyrolysis products provides insight into the relationship between the SP-AMS and AMS data, in particular the excellent correlation between the two sets of mass spectra in spite of the SP-AMS signals being frequently higher (Figs. 5b–c and 6b–d).

The excellent mass-spectral correlation is much better than expected given the possibility of different vaporization temperatures in SP-AMS and AMS (Sect. 2.2). Differences in vaporization temperature have previously been invoked to explain fragmentation differences in the SP-AMS relative to the AMS for OM coatings of diesel-exhaust soot and of a branched-chain laboratory diester (Onasch et al., 2012). Since fresh diesel-exhaust-soot coatings consist mostly of lubricating oil (Canagaratna et al., 2004; Massoli et al., 2012; Dallmann et al., 2014; Worton et al., 2014), both of these samples are chemically distinct from pyrolysis-generated OM. The similarity in AMS and SP-AMS pyrolysis-OM mass spectra may be due to fact that pyrolysis products have already undergone thermal bond rearrangement and dehydration reactions (Shafizadeh, 1984) and are thus less likely to do so when heated in the AMS or SP-AMS.

The higher SP-AMS signals in the OM time series in Fig. 5b–c might be hypothesized to reflect a difference in the SP-AMS sensitivity to OM when it is internally mixed with BC due to a change in either vaporization temperature or physical position of the vaporized particle (Sect. 2.3.5; Willis et al., 2014). However, this difference was observed even in the absence of rBC, as shown by the second fresh-emissions burn. In addition, the difference between SP-AMS and AMS was smaller for the aged-emissions experiment (Fig. 6b–c) than the fresh-emissions experiment (Fig. 5b–c). The apparent influence of aging is unlikely to be related to a change in mixing state: both aerodynamic- and mobility-size distributions were unimodal. A difference in particle focussing efficiency (Sect. 2.3.5) also does not explain the difference, as aging would have increased the size of the particles and therefore focussed a larger fraction of them into the SP-AMS laser. The difference between fresh and aged samples may therefore reflect an influence of the chemical composition of the OM.

It is therefore hypothesized that the observed discrepancy was caused by 1064 nm light-absorbing carbonaceous species other than rBC (brown carbon; Andreae and Gelencsér, 2006). Brown-carbon absorption would explain why the SP-AMS/AMS discrepancy was reduced after aging (Figs. 5b–c and 6b–c), since oxidation may reduce the conjugated or aromatic bonds required for light absorption. Lignin (Di Blasi, 2008) and its pyrolysis products (Simoneit et al., 1993) contain the majority of the aromatic species from wood and is itself brown (Andreae and Gelencsér, 2006). The water-soluble component of aerosol from inefficient beech-wood combustion is also brown (Klippel and Nussbaumer, 2007). Brown carbon would explain why the SP-AMS/AMS discrepancy in the aged experiment was highest for the anomalously high emissions of the second, failed-start burn (Fig. 6b and Fig. S2).

4.5 Refractory sources of potassium

Potassium ions, K^+, were observed as a dominant species in the SP-AMS mass spectrum but were negligible in the AMS. The SP-AMS therefore provides the possibility to specifically measure rBC-bound K^+ with high sensitivity, allowing its use as an atmospheric tracer for biomass-combustion aerosols. The requirement of internal mixing with rBC would avoid interference from other atmospheric sources of potassium like dust, vegetative debris, and sea salt (Andreae, 1983; Aiken et al., 2010), although a minor contribution to K^+ from vehicular emissions may be expected (Dallmann et al., 2014).

4.6 Refractory sources of water

As discussed in Sect. 2.2, H_2O^+ quantification in the SP-AMS is routinely confounded by background signals from water vapour and particulate water. The size-resolving PToF mode of the SP-AMS was used to separate these background signals from particulate signals, which was only possible when mass loadings were sufficiently high (Fig. S8). The particulate H_2O^+ signals were virtually negligible in the AMS but extremely high in the SP-AMS: a factor of 40 higher than C_3^+ (even after including the C_3^+ RIE; Sect. 2.3) during the flaming phase. Unlike CO_x^+, the H_2O^+ intensity did not change after aging and was constant (when normalized to C_3^+) to within 10 % between fresh and aged experiments.

The fact that the relative amount of H_2O^+ did not change after aging suggests that the dominant source was not surface functional groups (Smith and Chughtai, 1997). Rather,

Table 2. Uncentred correlations, excluding H_xO^+, of the OM mass spectra from PMF with literature AMS spectra (Aiken et al., 2007; Ulbrich et al., 2009, 2014). Correlations over 0.75 are highlighted.

		SP-AMS POM–Start	SP-AMS POM–Flame	AMS POM–Start	AMS POM–Flame
Levoglucosan		**0.78**	0.41	0.72	0.59
	m/z>44	**0.84**	0.58	**0.84**	0.55
Lignin-c.*		0.70	0.56	0.63	0.60
	m/z>44	0.71	**0.80**	0.74	**0.79**

* Lignin-c.: OM from the combustion of pure lignin; lignin in wood may pyrolyze differently (Di Blasi, 2008).

the large amount of H_2O^+ observed and its thermal stability in the AMS point towards an origin of liquid water adsorbed in pores on the BC itself (Popovitcheva et al., 2000). Such water may have been produced during combustion or evaporated from the logs, which had a moisture content of 12–20 % according to Swiss testing standards. Such adsorbed water is known to be thermally stable (Popovitcheva et al., 2000) and does not evaporate easily due to the inverse Kelvin effect (Marcolli, 2014).

Marcolli (2014) has proposed that the nucleation of ice on soot particles which are not immersed in water droplets (deposition-mode nucleation) is governed by such in-pore water. In a study of deposition-mode ice nucleation on beech-wood soot produced by a stove similar to ours, as well as diesel soot, Chou et al. (2013) found that oxidative aging did not influence the ice-nucleating activity of the soot particles, although the activity of the diesel and wood soot particles was different. Our observation that the H_2O^+ signal was unchanged upon aging is consistent with those results and suggests that the SP-AMS H_2O^+ signals may relate to the ice-nucleating potential of a given soot sample. More work is needed to explore this hypothesis.

5 Summary and conclusions

Dual-vaporizer aerosol-particle mass spectrometry was used to investigate the composition of beech-wood soot as a function of combustion time and simulated atmospheric aging. Vaporization via contact with an 873 K vaporizer (AMS) or via radiative heating by a 1064 nm continuous-wave laser (SP-AMS) allowed either the OM component of the particles or the entire soot particles to be probed, respectively.

The repeated addition of new logs to the wood stove led to a natural definition of a "starting" and "flaming" phase of combustion. The starting phase of combustion generated large amounts of OM with a similar mass spectrum in both AMS and SP-AMS. Analysis of the starting-phase mass spectrum showed that it was very similar to levoglucosan, indicating that the OM was dominated by the products of holocellulose pyrolysis. The corresponding flaming-phase OM appeared to consist of a mixture of holocellulose and lignin pyrolysis. These flaming-phase OM signals were virtually negligible relative to signals from refractory black carbon.

The near-absence of AMS signals during flaming combustion allowed refractory sources of signals in the SP-AMS to be distinguished. These signals were dominated by C_{1-3}^+, CO_{1-2}^+, and K^+. The ratio $C_4^+ : C_3^+$ was within the range reported by previous studies for mass-spectrally similar rBC samples.

Factor analysis showed that the refractory, oxygenated carbonaceous ions, rCO_x^+, were strongly associated with the rBC ions (C_x^+). Moreover, rCO_x^+ signals increased upon oxidation relative to C_x^+, and the CO_2^+ increased relative to CO^+. It was thus inferred that BC surface groups were the source of the rCO_x^+ signals. The degree of BC surface oxidation did not vary for different stages of the burn in either the fresh or aged aerosols and did not appear to be dependent on the concentration of co-emitted organics. For slightly or moderately aged aerosols, these conclusions may not hold and should be explored in future work. To our knowledge, these are the first measurements to address the surface oxidation of BC in the presence of co-emitted gases.

Significant signals from K and from H_2O were generated by soot particles in the SP-AMS only. The potassium signals would allow the SP-AMS to differentiate biomass-combustion soot from other sources in the atmosphere. The water signals did not change with oxidation, as would be expected had they originated from thermal-decomposition reactions and were much higher in signal than CO_x^+. They were therefore inferred to have originated from pores in the BC itself (Popovitcheva et al., 2000), which have been implicated in the heterogeneous ice-nucleating activity of soot (Marcolli, 2014).

These results indicate that wood-combustion soot is significantly oxygenated and contains OM impurities of similar chemical composition to the wood itself. The hygroscopicity, CCN activity, heterogeneous chemistry, and ice-nucleating behaviour of this soot (when either fresh or aged) are therefore likely to be different than that of laboratory surrogates. However, as only one fuel has been studied under controlled conditions in this work, more data are needed to constrain the compositional properties of biomass-combustion soot.

The Supplement related to this article is available online at doi:10.5194/acp-15-11885-2015-supplement.

Acknowledgements. The authors are grateful to Josef Wüest, Erich Wildhaber, and Martin Büchler for their support during the measurement campaign. This work was supported by the Swiss National Science Foundation, the Swiss Federal Offices for Energy (SFOE) and Environment (FOEN), and the OPTIWARES project of the Competence Centers for Environment and Sustainability (CCES) and Energy and Mobility (CCEM) of the ETH Zürich.

Edited by: D. Knopf

References

Aiken, A. C., DeCarlo, P. F., and Jimenez, J. L.: Elemental analysis of organic species with electron ionization high-resolution mass spectrometry, Anal. Chem., 79, 8350–8358, doi:10.1021/ac071150w, 2007.

Aiken, A. C., DeCarlo, P. F., Kroll, J. H., Worsnop, D. R., Huffman, J. A., Docherty, K. S., Ulbrich, I. M., Mohr, C., Kimmel, J. R., and Sueper, D.: O/C and OM/OC ratios of primary, secondary, and ambient organic aerosols with high-resolution time-of-flight aerosol mass spectrometry, Environ. Sci. Technol., 42, 4478–4485, doi:10.1021/es703009q, 2008.

Aiken, A. C., de Foy, B., Wiedinmyer, C., DeCarlo, P. F., Ulbrich, I. M., Wehrli, M. N., Szidat, S., Prevot, A. S. H., Noda, J., Wacker, L., Volkamer, R., Fortner, E., Wang, J., Laskin, A., Shutthanandan, V., Zheng, J., Zhang, R., Paredes-Miranda, G., Arnott, W. P., Molina, L. T., Sosa, G., Querol, X., and Jimenez, J. L.: Mexico city aerosol analysis during MILAGRO using high resolution aerosol mass spectrometry at the urban supersite (T0) – Part 2: Analysis of the biomass burning contribution and the non-fossil carbon fraction, Atmos. Chem. Phys., 10, 5315–5341, doi:10.5194/acp-10-5315-2010, 2010.

Akagi, S. K., Craven, J. S., Taylor, J. W., McMeeking, G. R., Yokelson, R. J., Burling, I. R., Urbanski, S. P., Wold, C. E., Seinfeld, J. H., Coe, H., Alvarado, M. J., and Weise, D. R.: Evolution of trace gases and particles emitted by a chaparral fire in California, Atmos. Chem. Phys., 12, 1397–1421, doi:10.5194/acp-12-1397-2012, 2012.

Akhter, M. S., Chughtai, A. R., and Smith, D. M.: The structure of hexane soot II: extraction studies, Appl. Spectrosc., 39, 154–167, 1985a.

Akhter, M. S., Chughtai, A. R., and Smith, D. M.: The structure of hexane soot I: spectroscopic studies, Appl. Spectrosc., 39, 143–153, 1985b.

Alcala-Jornod, C. and Rossi, M. J.: Chemical kinetics of the interaction of H_2O vapor with soot in the range $190\,K < T < 300\,K$: a diffusion tube study, J. Phys. Chem. A, 108, 10667–10680, doi:10.1021/jp040365w, 2004.

Alfarra, M. R., Coe, H., Allan, J. D., Bower, K. N., Boudries, H., Canagaratna, M. R., Jimenez, J. L., Jayne, J. T., Garforth, A. A., and Li, S.-M.: Characterization of urban and rural organic particulate in the lower Fraser valley using two aerodyne aerosol mass spectrometers, Atmos. Environ., 38, 5745–5758, doi:10.1016/j.atmosenv.2004.01.054, 2004.

Allan, J. D., Delia, A. E., Coe, H., Bower, K. N., Alfarra, M. R., Jimenez, J. L., Middlebrook, A. M., Drewnick, F., Onasch, T. B., and Canagaratna, M. R.: A generalised method for the extraction of chemically resolved mass spectra from aerodyne aerosol mass spectrometer data, J. Aerosol Sci., 35, 909–922, doi:10.1016/j.jaerosci.2004.02.007, 2004.

Andreae, M. O.: Soot carbon and excess fine potassium: long-range transport of combustion-derived aerosols, Science, 220, 1148–1151, doi:10.1126/science.220.4602.1148, 1983.

Andreae, M. O. and Gelencsér, A.: Black carbon or brown carbon? The nature of light-absorbing carbonaceous aerosols, Atmos. Chem. Phys., 6, 3131–3148, doi:10.5194/acp-6-3131-2006, 2006.

Attfield, M. D., Schleiff, P. L., Lubin, J. H., Blair, A., Stewart, P. A., Vermeulen, R., Coble, J. B., and Silverman, D. T.: The diesel exhaust in miners study: a cohort mortality study with emphasis on lung cancer, J. Natl. Cancer Inst., 104, 869–883, doi:10.1093/jnci/djs035, 2012.

Bond, T. C., Doherty, S. J., Fahey, D. W., Forster, P. M., Berntsen, T., DeAngelo, B. J., Flanner, M. G., Ghan, S., Kärcher, B., Koch, D., Kinne, S., Kondo, Y., Quinn, P. K., Sarofim, M. C., Schultz, M. G., Schulz, M., Venkataraman, C., Zhang, H., Zhang, S., Bellouin, N., Guttikunda, S. K., Hopke, P. K., Jacobson, M. Z., Kaiser, J. W., Klimont, Z., Lohmann, U., Schwarz, J. P., Shindell, D., Storelvmo, T., Warren, S. G., and Zender, C. S.: Bounding the role of black carbon in the climate system: a scientific assessment, J. Geophys. Res. Atmos., 118, 5380–5552, doi:10.1002/jgrd.50171, 2013.

Bond, T. C., Streets, D. G., Yarber, K. F., Nelson, S. M., Woo, J.-H., and Klimont, Z.: A technology-based global inventory of black and organic carbon emissions from combustion, J. Geophys. Res. Atmos., 109, D14203,, doi:10.1029/2003JD003697, 2004.

Brook, R. D., Rajagopalan, S., Pope, C. A., Brook, J. R., Bhatnagar, A., Diez-Roux, A. V., Holguin, F., Hong, Y., Luepker, R. V., and Mittleman, M. A.: Particulate matter air pollution and cardiovascular disease an update to the scientific statement from the American heart association, Circulation, 121, 2331–2378, doi:10.1161/CIR.0b013e3181dbece1, 2010.

Brunet, J., Fritz, Ö., and Richnau, G.: Biodiversity in European beech forests–a review with recommendations for sustainable forest management, Ecol. Bull, 53, 77–94, 2010.

Bruns, E. A., El Haddad, I., Keller, A., Klein, F., Kumar, N. K., Pieber, S. M., Corbin, J. C., Slowik, J. G., Brune, W. H., Baltensperger, U., and Prévôt, A. S. H.: Inter-comparison of laboratory smog chamber and flow reactor systems on organic aerosol yield and composition, Atmos. Meas. Tech., 8, 2315–2332, doi:10.5194/amt-8-2315-2015, 2015.

Cain, J. P., Gassman, P. L., Wang, H., and Laskin, A.: Micro-FTIR study of soot chemical composition–evidence of aliphatic hydrocarbons on nascent soot surfaces, Phys. Chem. Chem. Phys., 12, 5206, doi:10.1039/b924344e, 2010.

Cain, J. P., Camacho, J., Phares, D. J, Wang, H., and Laskin, A.: Evidence of aliphatics in nascent soot particles in premixed ethylene flames, Proc. Combust. Inst., 33, 533–540, doi:10.1016/j.proci.2010.06.164, 2011.

Canagaratna, M., Jayne, J., Jimenez, J., Allan, J., Alfarra, M., Zhang, Q., Onasch, T. B., Drewnick, F., Coe, H., Middle-

brook, A., Delia, A., Williams, L., Trimborn, A., Northway, M., DeCarlo, P., Kolb, C., Davidovits, P., and Worsnop, D.: Chemical and microphysical characterization of ambient aerosols with the aerodyne aerosol mass spectrometer, Mass Spectrom. Rev., 26, 185–222, doi:10.1002/mas.20115, 2007.

Canagaratna, M. R., Jayne, J. T., Ghertner, D. A., Herndon, S., Shi, Q., Jimenez, J. L., Silva, P. J., Williams, P., Lanni, T., Drewnick, F., Demerjian, K. L., Kolb, C. E., and Worsnop, D. R.: Chase studies of particulate emissions from in-use New York City vehicles, Aerosol Sci. Technol., 38, 555–573, doi:10.1080/02786820490465504, 2004.

Canagaratna, M. R., Massoli, P., Browne, E. C., Franklin, J. P., Wilson, K. R., Onasch, T. B., Kirchstetter, T. W., Fortner, E. C., Kolb, C. E, Jayne, J. T., Kroll, J. H., and Worsnop D. R.: Chemical compositions of black carbon particle cores and coatings via soot particle aerosol mass spectrometry with photoionization and electron ionization, J. Phys. Chem. A, doi:10.1021/jp510711u, 2015.

Cappa, C. D., Onasch, T. B., Massoli, P., Worsnop, D. R., Bates, T. S., Cross, E. S., Davidovits, P., Hakala, J., Hayden, K. L., and Jobson, B. T.: Radiative absorption enhancements due to the mixing state of atmospheric black carbon, Science, 337, 1078–1081, doi:10.1126/science.1223447, 2012.

Cappa, C. D., Onasch, T. B., Massoli, P., Worsnop, D. R., Bates, Timothy S and Cross, Eben S and Davidovits, P., Hakala, J., Hayden, K. L., and Jobson, B. T.: Response to comment on "Radiative Absorption Enhancements Due to the Mixing State of Atmospheric Black Carbon", Science, 339, 393–393, 2013.

Cappa, C. D., Williams, E. J., Lack, D. A., Buffaloe, G. M., Coffman, D., Hayden, K. L., Herndon, S. C., Lerner, B. M., Li, S.-M., Massoli, P., McLaren, R., Nuaaman, I., Onasch, T. B., and Quinn, P. K.: A case study into the measurement of ship emissions from plume intercepts of the NOAA ship *Miller Freeman*, Atmos. Chem. Phys., 14, 1337–1352, doi:10.5194/acp-14-1337-2014, 2014.

Chen, Q., Liu, Y., Donahue, N. M., Shilling, J. E., Martin, S. T.: Particle-phase chemistry of secondary organic material: modeled compared to measured O : C and H : C elemental ratios provide constraints, Environ. Sci. Technol., 45, 4763–4770, doi:10.1021/es104398s, 2011.

Chou, C., Kanji, Z. A., Stetzer, O., Tritscher, T., Chirico, R., Heringa, M. F., Weingartner, E., Prévôt, A. S. H., Baltensperger, U., and Lohmann, U.: Effect of photochemical ageing on the ice nucleation properties of diesel and wood burning particles, Atmos. Chem. Phys., 13, 761–772, doi:10.5194/acp-13-761-2013, 2013.

Corbin, J. C., Keller, A., Sierau, B., Lohmann, U., and Mensah, A. A.: Organic emissions from a wood stove and a pellet stove before and after simulated atmospheric aging, Aerosol Sci. Technol., 49, 1037–1050, doi:10.1080/02786826.2015.1079586, 2015a.

Corbin, J. C., Othman, A., Haskins, J. D., Mensah, A. A., Sierau, B., and Lohmann, U.: Peak fitting and integration uncertainties of the aerodyne aerosol mass spectrometer, Atmos. Meas. Tech. Discuss., 8, 3523–3523, doi:10.5194/amtd-8-3471-2015, 2015b.

Corbin, J. C., Sierau, B., Gysel, M., Laborde, M., Keller, A., Kim, J., Petzold, A., Onasch, T. B., Lohmann, U., and Mensah, A. A.: Mass spectrometry of refractory black carbon particles from six sources: carbon-cluster and oxygenated ions, Atmos. Chem. Phys., 14, 2591–2603, doi:10.5194/acp-14-2591-2014, 2015c.

Collier, S. and Zhang, Q.: Gas-Phase CO2 Subtraction for Improved Measurements of the Organic Aerosol Mass Concentration and Oxidation Degree by an Aerosol Mass Spectrometer, Environ. Sci. Technol., 47, 14324–14331, doi:10.1021/es404024h, 2013.

Cubison, M. J., Ortega, A. M., Hayes, P. L., Farmer, D. K., Day, D., Lechner, M. J., Brune, W. H., Apel, E., Diskin, G. S., Fisher, J. A.: Effects of aging on organic aerosol from open biomass burning smoke in aircraft and laboratory studies, Atmos. Chem. Phys., 11, 12049–12064, doi:10.5194/acp-11-12049-2011, 2011.

Cubison, M. J. and Jimenez, J. L.: Statistical precision of the intensities retrieved from constrained fitting of overlapping peaks in high-resolution mass spectra, Atmos. Meas. Tech., 8, 2333–2345, doi:10.5194/amt-8-2333-2015, 2015.

D'Anna, A.: Combustion-formed nanoparticles, Proc. Combust. Inst., 32, 593–613, doi:10.1016/j.proci.2008.09.005, 2009.

Dallmann, T. R., Onasch, T. B., Kirchstetter, T. W., Worton, D. R., Fortner, E. C., Herndon, S. C., Wood, E. C., Franklin, J. P., Worsnop, D. R., Goldstein, A. H., and Harley, R. A.: Characterization of particulate matter emissions from on-road gasoline and diesel vehicles using a soot particle aerosol mass spectrometer, Atmos. Chem. Phys., 14, 7585–7599, doi:10.5194/acp-14-7585-2014, 2014.

Daly, H. M. and Horn, A. B.: Heterogeneous chemistry of toluene, kerosene and diesel soots, Phys. Chem. Chem. Phys., 11, 1069–1076, doi:10.1039/B815400G, 2009.

Denier van der Gon, H. A. C., Bergström, R., Fountoukis, C., Johansson, C., Pandis, S. N., Simpson, D., and Visschedijk, A.: Particulate emissions from residential wood combustion in Europe – revised estimates and an evaluation, Atmos. Chem. Phys. Discuss., 14, 31719–31765, doi:10.5194/acpd-14-31719-2014, 2014.

Di Blasi, C.: Modeling chemical and physical processes of wood and biomass pyrolysis, Prog. Energy Combust. Sci., 34, 47–90, doi:10.1016/j.pecs.2006.12.001, 2008.

Dobbins, R. A.: Soot inception temperature and the carbonization rate of precursor particles, Combust. Flame, 130, 204–214, doi:10.1016/S0010-2180(02)00374-7, 2002.

Docherty, K. S., Jaoui, M., Corse, E., Jimenez, J. L., Offenberg, J. H., Lewandowski, M., and Kleindienst, T. E.: Collection Efficiency of the Aerosol Mass Spectrometer for Chamber-Generated Secondary Organic Aerosols, Aerosol Sci. Technol., 47, 294–309, doi:10.1080/02786826.2012.752572, 2013.

Donahue, N. M., Kroll, J. H., Pandis, S. N., and Robinson, A. L.: A two-dimensional volatility basis set – Part 2: Diagnostics of organic-aerosol evolution, Atmos. Chem. Phys., 12, 615–634, doi:10.5194/acp-12-615-2012, 2012.

Drewnick, F., Hings, S. S., Curtius, J., Eerdekens, G., and Williams, J.: Measurement of fine particulate and gas-phase species during the New Year's fireworks 2005 in Mainz, Germany, Atmos. Environ., 40, 4316–4327, doi:10.1016/j.atmosenv.2006.03.040, 2006.

Duplissy, J., DeCarlo, P. F., Dommen, J., Alfarra, M. R., Metzger, A., Barmpadimos, I., Prevot, A. S. H., Weingartner, E., Tritscher, T., Gysel, M., Aiken, A. C., Jimenez, J. L., Canagaratna, M. R., Worsnop, D. R., Collins, D. R., Tomlinson, J., and Baltensperger, U.: Relating hygroscopicity and composition of or-

ganic aerosol particulate matter, Atmos. Chem. Phys., 11, 1155–1165, doi:10.5194/acp-11-1155-2011, 2011.

Elsasser, M., Busch, C., Orasche, J., Schön, C., Hartmann, H., Schnelle-Kreis, J., and Zimmermann, R.: Dynamic changes of the aerosol composition and concentration during different burning phases of wood combustion, Energ. Fuels, 27, 4959–4968, doi:10.1021/ef400684f, 2013.

Engelhart, G. J., Hennigan, C. J., Miracolo, M. A., Robinson, A. L., and Pandis, S. N.: Cloud condensation nuclei activity of fresh primary and aged biomass burning aerosol, Atmos. Chem. Phys., 12, 7285–7293, doi:10.5194/acp-12-7285-2012, 2012.

Eriksson, A. C., Nordin, E. Z., Nyström, R., Pettersson, E., Swietlicki, E., Bergvall, C., Westerholm, R., Boman, C., and Pagels, J. H.: Particulate PAH emissions from residential biomass combustion: time-resolved analysis with aerosol mass spectrometry, Environ. Sci. Technol., 48, 7143–7150, doi:10.1021/es500486j, 2014.

Figueiredo, J. L., Pereira, M. F. R, Freitas, M. M. A., and Órfão, J. J. M.: Modification of the surface chemistry of activated carbons, Carbon, 37, 1379–1389, doi:10.1016/S0008-6223(98)00333-9, 1999.

Figueiredo, J. L., Pereira, M. F. R, Freitas, M. M. A., and Órfão, J. J. M.: Characterization of active sites on carbon catalysts, Ind. Eng. Chem. Res., 46, 4110–4115, doi:10.1021/ie061071v, 2007.

Fine, P. M., Cass, G. R., and Simoneit, B. R. T.: Chemical characterization of fine particle emissions from fireplace combustion of woods grown in the northeastern US, Environ. Sci. Technol., 35, 2665–2675, doi:10.1021/es001466k, 2001.

Fortner, E. C., Brooks, W. A., Onasch, T. B., Canagaratna, M. R., Massoli, P., Jayne, J. T., Franklin, J. P., Knighton, W. B., Wormhoudt, J., and Worsnop, D. R., Kolb, C. E., and Herndon, S. C.: Particulate emissions measured during the TCEQ comprehensive flare emission study, Ind. Eng. Chem. Res., 51, 12586–12592, doi:10.1021/ie202692y, 2012.

Fountoukis, C., Butler, T., Lawrence, M. G., Denier van der Gon, H. A. C., Visschedijk, A. J. H., Charalampidis, P., Pilinis, C., and Pandis, S. N.: Impacts of controlling biomass burning emissions on wintertime carbonaceous aerosol in Europe, Atmos. Environ., 175–182, doi:10.1016/j.atmosenv.2014.01.016, 2014.

Frenklach, M.: Reaction mechanism of soot formation in flames, Phys. Chem. Chem. Phys., 4, 2028–2037, 2002.

Genuit, W., Boon, J. J., and Faix, O.: Characterization of beech milled wood lignin by pyrolysis-gas chromatography-photoionization mass spectrometry, Anal. Chem., 59, 508–513, doi:10.1021/ac00130a029, 1987.

Glassman, I. and Yetter, R. A.: Combustion, Academic Press, Burlington, MA, USA, 2008.

Grieshop, A. P., Donahue, N. M., and Robinson, A. L.: Laboratory investigation of photochemical oxidation of organic aerosol from wood fires 2: analysis of aerosol mass spectrometer data, Atmos. Chem. Phys., 9, 2227–2240, doi:10.5194/acp-9-2227-2009, 2009.

Gysel, M., Laborde, M., Mensah, A. A., Corbin, J. C., Keller, A., Kim, J., Petzold, A., and Sierau, B.: Technical Note: The single particle soot photometer fails to reliably detect PALAS soot nanoparticles, Atmos. Meas. Tech., 5, 3099–3107, doi:10.5194/amt-5-3099-2012, 2012.

Han, C., Liu, Y., and He, H.: Role of organic carbon in heterogeneous reaction of NO_2 with soot, Environ. Sci. Technol., 47, 3174–3181, doi:10.1021/es304468n, 2013.

Han, C., Liu, Y., Ma, J., and He, H.: Effect of soot microstructure on its ozonization reactivity, J. Chem. Phys., 137, 084507, doi:10.1063/1.4747190, 2012a.

Han, C., Liu, Y., Ma, J., and He, H.: Key role of organic carbon in the sunlight-enhanced atmospheric aging of soot by O_2, Proc. Natl. Acad. Sci. USA, 109, 21250–21255, doi:10.1073/pnas.1212690110, 2012b.

Heal, M. R, Kumar, P., and Harrison, R. M.: Particles, air quality, policy and health, Chem. Soc. Rev., 41, 6606–6630, doi:10.1039/c2cs35076a, 2012.

Heidenreich, R. D., Hess, W. M., and Ban, L. L.: A test object and criteria for high resolution electron microscopy, J. Appl. Cryst., 1, 1–19, doi:10.1107/s0021889868004930, 1968.

Hennigan, C. J., Miracolo, M. A., Engelhart, G. J., May, A. A., Presto, A. A., Lee, T., Sullivan, A. P., McMeeking, G. R., Coe, H., Wold, C. E., Hao, W.-M., Gilman, J. B., Kuster, W. C., de Gouw, J., Schichtel, B. A., Collett Jr., J. L., Kreidenweis, S. M., and Robinson, A. L.: Chemical and physical transformations of organic aerosol from the photo-oxidation of open biomass burning emissions in an environmental chamber, Atmos. Chem. Phys., 11, 7669–7686, doi:10.5194/acp-11-7669-2011, 2011.

Hennigan, C. J., Sullivan, A. P., Collett, J. L., and Robinson, A. L.: Levoglucosan stability in biomass burning particles exposed to hydroxyl radicals, Geophys. Res. Lett., 37, L09806, doi:10.1029/2010gl043088, 2010.

Heringa, M. F., DeCarlo, P. F., Chirico, R., Tritscher, T., Dommen, J., Weingartner, E., Richter, R., Wehrle, G., Prévôt, A. S. H., and Baltensperger, U.: Investigations of primary and secondary particulate matter of different wood combustion appliances with a high-resolution time-of-flight aerosol mass spectrometer, Atmos. Chem. Phys., 11, 5945–5957, doi:10.5194/acp-11-5945-2011, 2011.

Holder, A. L., Carter, B. J., Goth-Goldstein, R., Lucas, D., and Koshland, C. P.: Increased cytotoxicity of oxidized flame soot, Atmos. Polut. Res., 3, 25–31, doi:10.5094/APR.2012.001, 2012.

Hopke, P. K.: A guide to positive matrix factorization, Workshop on UNMIX and PMF as Applied to $PM_{2.5}$, Research Triangle Park, NC, USA, edited by: Willis, R. D., available at: http://www.epa.gov/ttnamti1/files/ambient/pm25/workshop/laymen.pdf (last access: March 2015), 2000.

Hopkins, R. J., Tivanski, A. V., Marten, B. D., and Gilles, M. K.: Chemical bonding and structure of black carbon reference materials and individual carbonaceous atmospheric aerosols, J. Aerosol Sci., 38, 573–591, doi:10.1016/j.jaerosci.2007.03.009, 2007.

Huffman, J. A., Jayne, J. T., Drewnick, F., Aiken, A. C., Onasch, T. B., Worsnop, D. R., and Jimenez, J. L.: Design, modeling, optimization, and experimental tests of a particle beam width probe for the Aerodyne aerosol mass spectrometer, Aerosol Sci. Technol., 39, 1143–1163, doi:10.1080/02786820500423782, 2005.

Jacobson, M. Z.: Strong radiative heating due to the mixing state of black carbon in atmospheric aerosols, Nature, 409, 695–697, doi:10.1038/35055518, 2001.

Jacobson, M. Z.: Comment on "Radiative Absorption Enhancements Due to the Mixing State of Atmospheric Black Carbon", Science, 339, 393–393, 2013.

Jimenez, J. L., Jayne, J. T., Shi, Q., Kolb, C. E., Worsnop, D. R., Yourshaw, I., Seinfeld, J. H., Flagan, R. C., Zhang, X., Smith, K. A., Morris, J. W., and Davidovits, P.: Ambient aerosol sampling using the Aerodyne Aerosol Mass Spectrometer, J. Geophys. Res., 108, 8425, doi:10.1029/2001JD001213, 2003.

Jimenez, J. L., Canagaratna, M. R., Donahue, N. M., Prévôt, A. S. H., Zhang, Q., Kroll, J. H., DeCarlo, P. F., Allan, J. D., Coe, H., Ng, N. L., Aiken, A. C., Docherty, K. S., Ulbrich, I. M., Grieshop, A. P., Robinson, A. L., Duplissy, J., Smith, J. D., Wilson, K. R., Lanz, V. A., Hueglin, C., Sun, Y. L., Tian, J., Laaksonen, A., Raatikainen, T., Rautiainen, J., Vaattovaara, P., Ehn, M., Kulmala, M., Tomlinson, J. M., Collins, D. R., Cubison, M. J. E., Dunlea, J., Huffman, J. A., Onasch, T. B., Alfarra, M. R., Williams, P. I., Bower, K., Kondo, Y., Schneider, J., Drewnick, F., Borrmann, S., Weimer, S., Demerjian, K., Salcedo, D., Cottrell, L., Griffin, R., Takami, A., Miyoshi, T., Hatakeyama, S., Shimono, A., Sun, J. Y., Zhang, Y. M., Dzepina, K., Kimmel, J. R., Sueper, D., Jayne, J. T., Herndon, S. C., Trimborn, A. M., Williams, L. R., Wood, E. C., Middlebrook, A. M., Kolb, C. E., Baltensperger, U., and Worsnop, D. R.: Evolution of organic aerosols in the atmosphere, Science, 326, 1525–1529, doi:10.1126/science.1180353, 2009.

Jolleys, M. D., Coe, H., McFiggans, G., Capes, G., Allan, J. D., Crosier, J., Williams, P. I., Allen, G., Bower, K. N., Jimenez, J. L., Russell, L. M., Grutter, M., and Baumgardner, D.: Characterizing the aging of biomass burning organic aerosol by use of mixing ratios: a meta-analysis of four regions, Environ. Sci. Technol., 46, 13093–13102, doi:10.1021/es302386v, 2012.

Keller, A. and Burtscher, H.: A continuous photo-oxidation flow reactor for a defined measurement of the SOA formation potential of wood burning emissions, J. Aerosol Sci., 49, 9–20, doi:10.1016/j.jaerosci.2012.02.007, 2012.

Kiendler-Scharr, A., Zhang, Q., Hohaus, T., Kleist, E., Mensah, A., Mentel, T. F., Spindler, C., Uerlings, R., Tillmann, R., and Wildt, J.: Aerosol mass spectrometric features of biogenic SOA.: observations from a plant chamber and in rural atmospheric environments, Environ. Sci. Technol., 43, 8166–8172, doi:10.1021/es901420b, 2009.

Klippel, N. and Nussbaumer, T.: Wirkung von Verbrennungspartikeln – Vergleich der Unweltrelevanz von Holzfeuerungen und Dieselmotoren, Bundesamt für Energie und Bundesamt für Umwelt: Switzerland, 2007.

Knopf, D. A., Forrester, S. M., and Slade, J. H.: Heterogeneous oxidation kinetics of organic biomass burning aerosol surrogates by O_3, NO_2, N_2O_5, and NO_3, Phys. Chem. Chem. Phys., 13, 21050–21062, 2011.

Kolb, C. E., Cox, R. A., Abbatt, J. P. D., Ammann, M., Davis, E. J., Donaldson, D. J., Garrett, B. C., George, C., Griffiths, P. T., Hanson, D. R., Kulmala, M., McFiggans, G., Pöschl, U., Riipinen, I., Rossi, M. J., Rudich, Y., Wagner, P. E., Winkler, P. M., Worsnop, D. R., and O' Dowd, C. D.: An overview of current issues in the uptake of atmospheric trace gases by aerosols and clouds, Atmos. Chem. Phys., 10, 10561–10605, doi:10.5194/acp-10-10561-2010, 2010.

Kuwata, M., Kondo, Y., and Takegawa, N.: Critical condensed mass for activation of black carbon as cloud condensation nuclei in Tokyo, J. Geophys. Res. Atmos., 114, doi:10.1029/2009JD012086, 2009.

de Laeter, J. R., Böhlke, J. K., De Bièvre, P., Hidaka, H., Peiser, H. S., Rosman, K. J. R, and Taylor, P. D. P.: Atomic weights of the elements, review 2000 (IUPAC Technical Report), Pure Appl. Chem., 75, 683–800, doi:10.1351/pac200375060683, 2003.

Lamberg, H., Nuutinen, K., Tissari, J., Ruusunen, J., Yli-Pirilä, P., Sippula, O., Tapanainen, M., Jalava, P., Makkonen, U., and Teinilä, K.: Physicochemical characterization of fine particles from small-scale wood combustion, Atmos. Environ., 45, 7635–7643, doi:10.1016/j.atmosenv.2011.02.072, 2011.

Lanz, V. A., Alfarra, M. R., Baltensperger, U., Buchmann, B., Hueglin, C., and Prévôt, A. S. H.: Source apportionment of submicron organic aerosols at an urban site by factor analytical modelling of aerosol mass spectra, Atmos. Chem. Phys., 7, 1503–1522, doi:10.5194/acp-7-1503-2007, 2007.

Lee, T., Sullivan, A. P., Mack, L., Jimenez, J. L., Kreidenweis, S. M., Onasch, T. B., Worsnop, D. R., Malm, W., Wold, C. E, and Hao, W. M.: Chemical smoke marker emissions during flaming and smoldering phases of laboratory open burning of wildland fuels, Aerosol Sci. Technol., 44, i–v, doi:10.1080/02786826.2010.499884, 2010.

Leskinen, J., Ihalainen, M., Torvela, T., Kortelainen, M., Lamberg, H., Tiitta, P., Jakobi, G., Grigonyte, J., Joutsensaari, J., Sippula, O. and Tissari, J., and Virtanen, A., and Zimmermann, R., and Jokiniemi, J.: Effective density and morphology of particles emitted from small-scale combustion of various wood fuels, Environ. Sci. Technol., 48, 13298–13306, doi:10.1021/es502214a, 2014.

Li, Q., Shang, J., and Zhu, T.: Physicochemical characteristics and toxic effects of ozone-oxidized black carbon particles, Atmos. Environ., 81, 68–75, doi:10.1016/j.atmosenv.2013.08.043, 2013.

Lighty, J. S., Veranth, J. M., and Sarofim, A. F.: Combustion aerosols: factors governing their size and composition and implications to human health, JAPCA J. Air Waste Ma., 50, 1565–1618, 2000.

Lipsky, E. M. and Robinson, A. L.: Effects of dilution on fine particle mass and partitioning of semivolatile organics in diesel exhaust and wood smoke, Environ. Sci. Technol., 40, 155–162, doi:10.1021/es050319p, 2006.

Liu, J., Fan, S., Horowitz, L. W., and Levy, H.: Evaluation of factors controlling long-range transport of black carbon to the Arctic, J. Geophys. Res. Atmos., 116, D04307, doi:10.1029/2010JD015145, 2011.

Liu, D., Allan, J., Whitehead, J., Young, D., Flynn, M., Coe, H., McFiggans, G., Fleming, Z. L., and Bandy, B.: Ambient black carbon particle hygroscopic properties controlled by mixing state and composition, Atmos. Chem. Phys., 13, 2015–2029, doi:10.5194/acp-13-2015-2013, 2013.

Marcolli, C.: Deposition nucleation viewed as homogeneous or immersion freezing in pores and cavities, Atmos. Chem. Phys., 14, 2071–2104, doi:10.5194/acp-14-2071-2014, 2014.

Martin, M., Tritscher, T., Jurányi, Z., Heringa, M. F., Sierau, B., Weingartner, E., Chirico, R., Gysel, M., Prévôt, A. S. H., and Baltensperger, U.: Hygroscopic properties of fresh and aged wood burning particles, J. Aerosol Sci., 56, 15–29, doi:10.1016/j.jaerosci.2012.08.006, 2012.

Massoli, P., Fortner, E. C., Canagaratna, M. R., Williams, L. R., Zhang, Q., Sun, Y., Schwab, J. J., Trimborn, A., Onasch, T. B., and Demerjian, K. L.: Pollution gradients and chemical char-

acterization of particulate matter from vehicular traffic near major roadways: results from the 2009 Queens College Air Quality study in NYC, Aerosol Sci. Technol., 46, 1201–1218, doi:10.1080/02786826.2012.701784, 2012.

Matthew, B. M., Middlebrook, A. M., and Onasch, T. B.: Collection efficiencies in an Aerodyne Aerosol Mass Spectrometer as a function of particle phase for laboratory generated aerosols, Aerosol Sci. Technol., 42, 884–898, doi:10.1080/02786820802356797, 2008.

McLafferty, F. W. and Tureček, F.: Interpretation of Mass Spectra, 1993, University Science Books, Sausalito, California, 1993.

McWhinney, R. D., Gao, S. S., Zhou, S., and Abbatt, J. P. D.: Evaluation of the effects of ozone oxidation on redox-cycling activity of two-stroke engine exhaust particles, Environ. Sci. Technol., 45, 2131–2136, doi:10.1021/es102874d, 2011.

McWhinney, R. D., Badali, K., Liggio, J., Li, S.-M., and Abbatt, J. P. D.: Filterable redox cycling activity: a comparison between diesel exhaust particles and secondary organic aerosol constituents, Environ. Sci. Technol., 47, 3362–3369, doi:10.1021/es304676x, 2013.

Middlebrook, A. M., Bahreini, R., Jimenez, J. L., and Canagaratna, M. R.: Evaluation of composition-dependent collection efficiencies for the Aerodyne aerosol mass spectrometer using field data, Aerosol Sci. Technol., 46, 258–271, doi:10.1080/02786826.2011.620041, 2012.

Mikhailov, E. F., Vlasenko, S. S., Podgorny, I. A., Ramanathan, V., and Corrigan, C. E.: Optical properties of soot–water drop agglomerates: an experimental study, J. Geophys. Res., 111, D07209, doi:10.1029/2005JD006389, 2006.

Monge, M. E., D'Anna, B., Mazri, L., Giroir-Fendler, A., Ammann, M., Donaldson, D. J., and George, C.: Light changes the atmospheric reactivity of soot, Proc. Natl. Acad. Sci. USA, 107, 6605–6609, doi:10.1073/pnas.0908341107, 2010.

Moteki, N. and Kondo, Y.: Dependence of laser-induced incandescence on physical properties of black carbon aerosols: measurements and theoretical interpretation, Aerosol Sci. Technol., 44, 663–675, doi:10.1080/02786826.2010.484450, 2010.

Mul, G., Neeft, J. P. A., Kapteijn, F., and Moulijn, J. A.: The formation of carbon surface oxygen complexes by oxygen and ozone, the effect of transition metal oxides, Carbon, 36, 1269–1276, doi:10.1016/S0008-6223(97)00209-1, 1998.

Ng, N. L., Canagaratna, M. R., Jimenez, J. L., Chhabra, P. S., Seinfeld, J. H., and Worsnop, D. R.: Changes in organic aerosol composition with aging inferred from aerosol mass spectra, Atmos. Chem. Phys., 11, 6465–6474, doi:10.5194/acp-11-6465-2011, 2011.

Onasch, T. B., Trimborn, A., Fortner, E. C., Jayne, J. T., Kok, G. L., Williams, L. R., Davidovits, P., and Worsnop, D. R.: Soot particle aerosol mass spectrometer: development, validation, and initial application, Aerosol Sci. Technol., 46, 804–817, doi:10.1080/02786826.2012.663948, 2012.

Ortega, A. M., Day, D. A., Cubison, M. J., Brune, W. H., Bon, D., de Gouw, J. A., and Jimenez, J. L.: Secondary organic aerosol formation and primary organic aerosol oxidation from biomass-burning smoke in a flow reactor during FLAME-3, Atmos. Chem. Phys., 13, 11551–11571, doi:10.5194/acp-13-11551-2013, 2013.

Paatero, P.: PMF User's Guide, University of Helsinki, Helsinki, 2000.

Paatero, P. and Hopke, P. K.: Discarding or downweighting high-noise variables in factor analytic models, Anal. Chim. Acta, 490, 277–289, doi:10.1016/S0003-2670(02)01643-4, 2003.

Paatero, P. and Tapper, U.: Positive matrix factorization: A non-negative factor model with optimal utilization of error estimates of data values, Environmetrics, 5, 111–126, doi:10.1002/env.3170050203, 1994.

Paatero, P., Hopke, P. K., Song, X.-H., and Ramadan, Z.: Understanding and controlling rotations in factor analytic models, Chemom. Intell. Lab. Syst., 60, 253–264, doi:10.1016/S0169-7439(01)00200-3, 2002.

Pan, C.-J. G., Schmitz, D. A., Cho, A. K., Froines, J., and Fukuto, J. M.: Inherent redox properties of diesel exhaust particles: catalysis of the generation of reactive oxygen species by biological reductants, Toxicol. Sci., 81, 225–232, doi:10.1093/toxsci/kfh199, 2004.

Petzold, A., Ogren, J. A., Fiebig, M., Laj, P., Li, S.-M., Baltensperger, U., Holzer-Popp, T., Kinne, S., Pappalardo, G., Sugimoto, N., Wehrli, C., Wiedensohler, A., and Zhang, X.-Y.: Recommendations for reporting "black carbon" measurements, Atmos. Chem. Phys., 13, 8365–8379, doi:10.5194/acp-13-8365-2013, 2013.

Polissar, A. V., Hopke, P. K., Paatero, P., Malm, W. C., and Sisler, J. F.: Atmospheric aerosol over Alaska, 2, elemental composition and sources, J. Geophys. Res. Atmos., 103, 19045–19057, doi:10.1029/98JD01212, 1998.

Popovitcheva, O. B., Persiantseva, N. M., Trukhin, M. E., Rulev, G. B., Shonija, N. K., Buriko, Y. Y., Starik, A. M., Demirdjian, B., Ferry, D., and Suzanne, J.: Experimental characterization of aircraft combustor soot: microstructure, surface area, porosity and water adsorption, Phys. Chem. Chem. Phys., 2, 4421–4426, doi:10.1039/B004345L, 2000.

Ramanathan, V. and Carmichael, G.: Global and regional climate changes due to black carbon, Nat. Geosci., 1, 221–227, doi:10.1038/ngeo156, 2008.

Reff, A., Eberly, S. I., and Bhave, P. V.: Receptor modeling of ambient particulate matter data using positive matrix factorization: review of existing methods, JAPCA J. Air Waste Ma., 57, 146–154, 2007.

Rogge, W. F., Hildemann, L. M., Mazurek, M. A., Cass, G. R., and Simoneit, B. R. T.: Sources of fine organic aerosol, 9, pine, oak, and synthetic log combustion in residential fireplaces, Environ. Sci. Technol., 32, 13–22, doi:10.1021/es960930b, 1998.

Schmidl, C., Marr, I. L., Caseiro, A., Kotianová, P., Berner, A., Bauer, H., Kasper-Giebl, A., and Puxbaum, H.: Chemical characterisation of fine particle emissions from wood stove combustion of common woods growing in mid-European Alpine regions, Atmos. Environ., 42, 126–141, doi:10.1016/j.atmosenv.2007.09.028, 2008.

Schmidt, M. W. I., Masiello, C. A., and Skjemstad, J. O.: Final recommendations for reference materials in black carbon analysis, Eos Trans. AGU, 84, 582–582, doi:10.1029/2003eo520006, 2003.

Schwarz, J. P., Gao, R. S., Fahey, D. W., Thomson, D. S., Watts, L. A., Wilson, J. C., Reeves, J. M., Darbeheshti, M., Baumgardner, D. G., Kok, G. L., Chung, S. H., Schulz, M., Hendricks, J., Lauer, A., Kärcher, B., Slowik, J. G., Rosenlof, K. H., Thompson, T. L., Langford, A. O., Loewenstein, M., Aikin, K. C.: Single-particle measurements of midlatitude

black carbon and light-scattering aerosols from the boundary layer to the lower stratosphere, J. Geophys. Res., 111, D16207, doi:10.1029/2006JD007076, 2006.

Shafizadeh, F.: The chemistry of pyrolysis and combustion, in: The Chemistry of Solid Wood, edited by: Rowell, R., Advances in Chemistry, American Chemical Society. Chem., Washington DC, USA, 489–529, doi:10.1021/ba-1984-0207.ch013, 1984.

Silverman, D. T., Samanic, C. M., Lubin, J. H., Blair, A. E., Stewart, P. A. Vermeulen, R., Coble, J. B., Rothman, N., Schleiff, P. L., and Travis, W. D.: The diesel exhaust in miners study: a nested case-control study of lung cancer and diesel exhaust, J. Natl. Cancer Inst., 104, 855–868, doi:10.1093/jnci/djs034, 2012.

Simoneit, B. R. T., Rogge, W. F., Mazurek, M. A., Standley, L. J., Hildemann, L. M., and Cass, G. R.: Lignin pyrolysis products, lignans, and resin acids as specific tracers of plant classes in emissions from biomass combustion, Environ. Sci. Technol., 27, 2533–2541, doi:10.1021/es00048a034, 1993.

Simoneit, B. R. T., Schauer, J. J., Nolte, C. G., Oros, D. R., Elias, V. O., Fraser, M. P., Rogge, W. F., and Cass, G. R.,: Levoglucosan, a tracer for cellulose in biomass burning and atmospheric particles, Atmos. Environ., 33, 173–182, doi:10.1016/s1352-2310(98)00145-9, 1999.

Simpson, D., Winiwarter, W., Börjesson, G., Cinderby, S., Ferreiro, A., Guenther, A., Hewitt, C. N., Janson, R., Khalil, M. A. K., Owen, S., Pierce, T. E., Puxbaum, H., Shearer, M., Skiba, U., Steinbrecher, R., Tarrasón, L., and Öquist, M. G.: Inventorying emissions from nature in Europe, J. Geophys. Res., 104, 8113–8152, doi:10.1029/98jd02747, 1999.

Slade, J. H. and Knopf, D. A.: Heterogeneous OH oxidation of biomass burning organic aerosol surrogate compounds: assessment of volatilisation products and the role of OH concentration on the reactive uptake kinetics, Phys. Chem. Chem. Phys., 15, 5898–5915, 2013.

Smith, D. M. and Chughtai, A. R.: The surface structure and reactivity of black carbon, Colloid. Surface. A., 105, 47–77, doi:10.1016/0927-7757(95)03337-1, 1995.

Smith, D. M. and Chughtai, A. R.: Photochemical effects in the heterogeneous reaction of soot with ozone at low concentrations, J. Atmos. Chem., 26, 77–91, doi:10.1023/a:1005702818675, 1997.

Sorensen, C. M.: The mobility of fractal aggregates: a review, Aerosol Sci. Technol., 45, 765–779, doi:10.1080/02786826.2011.560909, 2011.

Stanmore, B. R., Brilhac, J. F., and Gilot, P.: The oxidation of soot: a review of experiments, mechanisms and models, Carbon, 39, 2247–2268, doi:10.1016/S0008-6223(01)00109-9, 2001.

Sueper, D., Jimenez, J. L., Aiken, A., and DeCarlo, P.: PIKA ToF-AMS High Resolution Analysis Software, available at: http://cires1.colorado.edu/jimenez-group/wiki/index.php/ToF-AMS_Analysis_Software (last access: October 2015)„ 2011.

Sun, Y. L., Zhang, Q., Anastasio, C., and Sun, J.: Insights into secondary organic aerosol formed via aqueous-phase reactions of phenolic compounds based on high resolution mass spectrometry, Atmos. Chem. Phys., 10, 4809–4822, doi:10.5194/acp-10-4809-2010, 2010.

Szidat, S., Jenk, T. M., Synal, H.-A., Kalberer, M., Wacker, L., Hajdas, I., Kasper-Giebl, A., and Baltensperger, U.: Contributions of fossil fuel, biomass-burning, and biogenic emissions to carbonaceous aerosols in Zurich as traced by ^{14}C, J. Geophys. Res. Atmos., 111, doi:10.1029/2005JD006590, 2006.

Szidat, S., Prévôt, A. S. H., Sandradewi, J., Alfarra, M R., Synal, H.-A., Wacker, L., and Baltensperger, U.: Dominant impact of residential wood burning on particulate matter in Alpine valleys during winter, Geophys. Res. Lett., 34, L05820, doi:10.1029/2006GL028325, 2007.

Timell, T. E.: Recent progress in the chemistry of wood hemicelluloses, Wood Sci. Technol., 1, 45–70, doi:10.1007/BF00592255, 1967.

Torvela, T., Tissari, J., Sippula, O., Kaivosoja, T., Leskinen, J., Virén, A., Lähde, A., and Jokiniemi, J.: Effect of wood combustion conditions on the morphology of freshly emitted fine particles, Atmos. Environ., 87, 65–76, doi:10.1016/j.atmosenv.2014.01.028, 2014.

Tree, D. R. and Svensson, K. I.: Soot processes in compression ignition engines, Prog. Energy Combust. Sci., 33, 272–309, doi:10.1016/j.pecs.2006.03.002, 2007.

Tritscher, T., Jurányi, Z., Martin, M., Chirico, R., Gysel, M., Heringa, M. F., DeCarlo, P. F., Sierau, B., Prévôt, A. S. H., and Weingartner, E.: Changes of hygroscopicity and morphology during ageing of diesel soot, Environ. Res. Lett., 6, 034026, doi:10.1088/1748-9326/6/3/034026, 2011.

Ulbrich, I. M., Canagaratna, M. R., Zhang, Q., Worsnop, D. R., and Jimenez, J. L.: Interpretation of organic components from Positive Matrix Factorization of aerosol mass spectrometric data, Atmos. Chem. Phys., 9, 2891–2918, doi:10.5194/acp-9-2891-2009, 2009.

Ulbrich, I. M., Lechner, M., and Jimenez, J. L.: AMS Spectral Database, available at: http://cires.colorado.edu/jimenez-group/AMSsd/ last access: August 2014.

Vakkari, V., Kerminen, V.-M., Beukes, J. P., Tiitta, P., Zyl, P. G., Josipovic, M., Venter, A. D., Jaars, K., Worsnop, D. R., Kulmala, M. and, Laakso, L.: Rapid changes in biomass burning aerosols by atmospheric oxidation, Geophys. Res. Lett., 41, 2644–2651, doi:10.1002/2014GL059396, 2014.

Vernooij, M. G. C., Mohr, M., Tzvetkov, G., Zelenay, V., Huthwelker, T., Kaegi, R., Gehrig, R., and Grobéty, B.: On source identification and alteration of single diesel and wood smoke soot particles in the atmosphere; an X-ray microspectroscopy study, Environ. Sci. Technol., 43, 5339–5344, doi:10.1021/es800773h, 2009.

Wang H.: Formation of nascent soot and other condensed-phase materials in flames, Proc. Combust. Inst., 33, 41–67, doi:10.1016/j.proci.2010.09.009, 2011.

Weimer, S., Alfarra, M. R., Schreiber, D., Mohr, M., Prévôt, A. S. H., and Baltensperger, U.: Organic aerosol mass spectral signatures from wood-burning emissions: influence of burning conditions and wood type, J. Geophys. Res. Atmos., 113, D10, doi:10.1029/2007JD009309, 2008.

Westberg, H. M., Byström, M., and Leckner, B.: Distribution of potassium, chlorine, and sulfur between solid and vapor phases during combustion of wood chips and coal, Energy Fuels, 17, 18–28, doi:10.1021/ef020060l, 2003.

Willis, M. D., Lee, A. K. Y., Onasch, T. B., Fortner, E. C., Williams, L. R., Lambe, A. T., Worsnop, D. R., and Abbatt, J. P. D.: Collection efficiency of the soot-particle aerosol mass spectrometer (SP-AMS) for internally mixed particulate black carbon, At-

mos. Meas. Tech., 7, 4507–4516, doi:10.5194/amt-7-4507-2014, 2014.

Worton, D. R., Isaacman, G., Gentner, D. R., Dallmann, T. R., Chan, A. W. H., Ruehl, C. R, Kirchstetter, T., Wilson, K. R., Harley, R. A., and Goldstein, A. H.: Lubricating oil dominates primary organic aerosol emissions from motor vehicles, Environ. Sci. Technol., 48, 3698–3706, doi:10.1021/es405375j, 2014.

Yang, H., Yan, R., Chen, H., Lee, D. H., and Zheng, C.: Characteristics of hemicellulose, cellulose and lignin pyrolysis, Fuel, 86, 1781–1788, doi:10.1016/j.fuel.2006.12.013, 2007.

Zelenay, V., Mooser, R., Tritscher, T., Krepelová, A., Heringa, M. F., Chirico, R., Prévôt, A. S. H., Weingartner, E., Baltensperger, U., Dommen, J., Watts, B., Raabe, J., Huthwelker, T., and Ammann, M.: Aging induced changes on NEXAFS fingerprints in individual combustion particles, Atmos. Chem. Phys., 11, 11777–11791, doi:10.5194/acp-11-11777-2011, 2011.

Zhang, Q., Alfarra, M. R., Worsnop, D. R., Allan, J. D., Coe, H., Canagaratna, M. R., and Jimenez, J. L.: Deconvolution and quantification of hydrocarbon-like and oxygenated organic aerosols based on aerosol mass spectrometry, Environ. Sci. Technol., 39, 4938–4952, doi:10.1021/es048568l, 2005.

Zhang, Q., Jimenez, J. L., Canagaratna, M. R, Ulbrich, I. M., Ng, N. L., Worsnop, D. R., and Sun, Y.: Understanding atmospheric organic aerosols via factor analysis of aerosol mass spectrometry: a review, Anal. Bioanal. Chem., 401, 3045–3067, doi:10.1007/s00216-011-5355-y, 2011.

Zielke, U., Hüttinger, K. J., and Hoffman, W. P.: Surface-oxidized carbon fibers, I, surface structure and chemistry, Carbon, 34, 983–998, doi:10.1016/0008-6223(96)00032-2, 1996.